INSTITUTE OF PHYSICS PUBLISHING PLASMA PHYSICS AND CONTROLLED FUSION

Plasma Phys. Control. Fusion **47** (2005) 1709–1741 doi:10.1088/0741-3335/47/10/008

Improving tokamak vertical position control in the presence of power supply voltage saturation

J-Y Favez[1,2], J B Lister[1], Ph Müllhaupt[2] and B Srinivasan[2]

[1] Centre de Recherches en Physique des Plasmas, Association EURATOM-Confédération Suisse, EPFL, 1015 Lausanne, Switzerland
[2] Laboratoire d'Automatique, EPFL, 1015 Lausanne, Switzerland

E-mail: Jo.Lister@epfl.ch

Received 25 February 2005, in final form 21 June 2005
Published 16 September 2005
Online at stacks.iop.org/PPCF/47/1709

Abstract

The control of the current, position and shape of an elongated cross-section tokamak plasma is complicated by the so-called instability of the current vertical position. Linearized models all share the feature of a single unstable eigenmode, attributable to this vertical instability of the plasma equilibrium movement, and a large number of stable or marginally stable eigenmodes, attributable to zero or positive resistance in all other model circuit equations. Due to the size and therefore cost of the ITER tokamak, there will naturally be smaller margins in the poloidal field coil power supplies, implying that the feedback control will experience actuator saturation during large transients due to a variety of plasma disturbances. Current saturation is relatively benign, due to the integrating nature of the tokamak, resulting in a reasonable time horizon for strategically handling the approach to saturation which leads to the loss of one degree of freedom in the feedback control for each saturated coil. On the other hand, voltage saturation is produced by the feedback controller itself, with no intrinsic delay. This paper presents a feedback controller design approach which explicitly takes saturation of the power supply voltage into account when producing the power supply demand signals. We consider the vertically stabilizing part of the ITER controller (fast controller) with one power supply and therefore a single saturated input. We consider an existing ITER controller and enlarge its region of attraction to the full null controllable region by adding a continuous nonlinearity into the control. In a system with a single unstable eigenmode and a single stable eigenmode we have already provided a proof of the asymptotical stability of the closed loop system, and we have examined the performance of this new continuous nonlinear controller. We have subsequently extended this analysis to a system with a single eigenmode and multiple stable eigenmodes. The method requires state feedback control, and therefore a reconstruction of the states is indispensable. We discuss the feasibility of extracting these states from the available diagnostic information as well as other implementation details. As a complement to our ITER simulations

we confirm the enlargement of the region of attraction by the new controller by a JET simulation.

(Some figures in this article are in colour only in the electronic version)

1. Introduction

If the plasma cross-section of a tokamak plasma is elongated, the control of the current, position and shape of the plasma is complicated by the instability of the vertical position. This can be understood as the effect of a quadrupole field which stretches the current distribution in the vertical direction, generating an equilibrium which is attracted to either source of the quadrupole field if it departs from its equilibrium position, like a ball between two magnet poles. Alternatively, it can be considered as a lateral squeezing of the equilibrium, again leading to vertical instability, like squeezing an orange pip.

Elongation of the plasma shape is a feature of all modern tokamaks since it is necessary to optimize the use of the toroidal magnetic field so elongation will naturally be a feature of ITER. Considerable work has gone into modelling the current, position and shape control of ITER, demonstrating adequate controllability with a large variety of models and controller designs. Linearized equilibrium response models of the vertically elongated plasma, the surrounding passive structures and the poloidal field (PF) coils all share the feature of a single positive eigenvalue (attributable to the so-called vertical instability) and a large number of negative eigenvalues (attributable to positive resistance in all circuit equations). Existing experiments have exploited the control of vertically unstable plasmas with little difficulty. We summarize some of the models presently used in section 2.

Due to the large size and therefore large cost of the ITER project, there are inevitably smaller operating margins compared with the present experiments. The currents in the PF coils are large and limit the accessible equilibria. The voltages of the PF coil power supplies are the actuators of the plasma shape, position and current feedback control system and are limited to reduce the cost, insulation requirements and ac coupling losses in the superconducting magnets during feedback control. The implication of the reduction of the different operating margins is that the plasma shape, position and current feedback control loop may experience actuator saturation during large transients, due to a variety of frequent disturbances inside the plasma itself. Indeed, if there were no saturation, then the voltages should be considered to be over-designed. The PF coil saturation can be of two types, limiting the PF coil power supply voltage, or limiting the delivered electrical current in the PF coil. Saturation of the PF coil current is more benign, due to the integrating nature of the tokamak load, which is dominantly inductive. The PF coil currents cannot vary faster than the maximum applied voltages allow, resulting in a significant time horizon for strategically handling the approach to coil current saturation. On the other hand, voltage saturation is produced by the feedback controller itself, with no intrinsic delay.

The ITER PF coil voltage limits are derived from assumptions on the evolution of the scenario, on the noise in the feedback control loop and on disturbances to the plasma itself, such as changes in the plasma energy (expressed in linearized models as sudden changes in β_p, the ratio between kinetic pressure and poloidal magnetic energy) or to changes in the current profile (expressed in the same models as sudden changes in the internal inductance l_i). Typical examples of such disturbances are sawteeth, edge localized modes (ELMs) and minor disruptions [1].

If the scenario evolution, noise and disturbances combine to generate a PF coil demand voltage which is above the supply limit, the PF voltage will saturate and feedback control could be lost if the saturation persists. When this happens, the plasma will continue to move vertically in spite of the saturation. If the radial field amplifier current saturates, then the vertical displacement will grow with the open-loop growth rate. If the radial field amplifier voltage saturates, then the vertical displacement will grow slower than the open-loop growth rate but will nonetheless continue to grow. These two cases are generally referred to as vertical displacement events (VDEs). The moving plasma induces currents in all conducting structures, which may then be subject to large forces, depending on the local magnetic field. The loss of the plasma kinetic energy leads to a large thermal deposition on exposed surfaces, particularly the divertor plates, leading to thermo-mechanical forces and erosion. It is clear that the number of VDEs must be limited as much as possible, as part of the ITER design criteria.

The objective of this paper is to explore the design of a feedback controller which explicitly takes into consideration the saturation of the PF coil voltages when producing the voltage demand signals, thereby reducing the likely loss of control of the vertically unstable plasma position. A first attempt made during the original ITER design work in the mid-1990s was encouraging, but periodically failed. We have therefore revisited this issue, in view of its importance to ITER, taking a new formal approach. A summary of the new controller design is presented in sections 3 and 4, but without the full mathematical details. The result is a conceptually simple modification to any existing controller design. The approach makes use of the notion of the unstable state of the linearized model of the tokamak. Since the unstable state is not yet a commonly used concept in treating the vertical control problem in tokamaks, we discuss this in section 3. In section 4, we use the unstable state to derive an optimal modification to the design of the feedback controller, showing that without this modification, the control will always be sub-optimal. This approach is referred to as the 'continuous nonlinear global stabilizing controller' (CNGSC). In section 5, we test out the CNGSC in two different conditions. Firstly, we use a linearized model of ITER to demonstrate the performance enhancement in particular cases. Secondly, we use a linear model of JET, including the available magnetics diagnostics, to confirm the improvement on an existing device which, like ITER, relies on a single fast power supply for vertical stabilization. We test whether the unstable state can be measured in TCV. In section 6, we discuss the implementation for full discharge control and present our conclusions.

2. Modelling

As interest in modelling the combined plasma, vessel and PF coil system increased, many approaches were tried. Linearized models of the vertical instability were used during early JET operation, based on equivalent point currents to represent the stabilizing property of the vacuum vessel [2]. This was extended, for application to DIII-D, to an eigenmode approximation of the vessel description, retaining the first up–down asymmetric eigenmode of the vessel currents and exploring the controllability with a proportional-derivative (PD) feedback controller, both theoretically and experimentally [3, 4]. These approaches considered the plasma to be a filament. Deformation of the plasma equilibrium was considered in the CREATE-L model, used for the ITER design and validated experimentally on the TCV tokamak [5, 6]. A simpler enhanced rigid current displacement model (RZIP) was developed and validated for TCV, considering changes to the plasma current and to its radial position [7, 8]. A deformable plasma model was subsequently developed for TCV highly shaped plasmas with the highest growth rates [9]. This comprehensive set of linearized model categories is completed by nonlinear evolutionary models, solving the free-boundary equilibrium problem together with the plasma

Table 1. The physical state variables.

$I_a \in \mathbb{R}^{n_a}$	n_a active coil currents
$I_v \in \mathbb{R}^{n_v}$	n_v vessel eigenmode currents
$I_p \in \mathbb{R}$	Plasma current
$RI_{p_0} \in \mathbb{R}$	Radial plasma position times I_{p_0}
$zI_{p_0} \in \mathbb{R}$	Vertical plasma position times I_{p_0}

feedback control, typified by TSC [10] and DINA [11, 12]. This spectrum of approaches illustrates the tools we have available today, but we have not tried to review them here.

In this paper, we make use of the single vessel eigenmode representation [3] for its algebraic simplicity, of the linearized RZIP model [8] and of the linearized CREATE-L models for JET [13] and ITER [14]. A crucial feature of all these linearized models is the presence of a single positive eigenvalue when the vertical plasma position is unstable. This point is essential for the following argument. We first briefly recall these three models and their properties, and we subsequently extend them by introducing ELM-like disturbances.

2.1. Simple second order model of the vertical movement

In [3] the linearized tokamak model with the first up–down asymmetric vessel eigenmode and one voltage input feeding a serial connected up–down antisymmetric coil system was described by the algebraic equation defining the vertical position assuming instantaneous force-balance, for which the current-distribution-averaged radial field is zero and the plasma mass is neglected:

$$\alpha z I_{p_0} + M'_{vp} I_v + M'_{ap} I_a = 0 \tag{1}$$

and by the two differential circuit equations

$$L_a \dot{I}_a + \Omega_a I_a + M_{av} \dot{I}_v + M'_{az} \dot{z} I_{p_0} = V_a, \tag{2}$$

$$L_v \dot{I}_v + \Omega_v I_v + M_{av} \dot{I}_a + M'_{vz} \dot{z} I_{p_0} = 0, \tag{3}$$

where all variables are small variations about the linearization point. Throughout this paper, we denote scalar and vector quantities by lower case and matrices by upper case, with the exception of the standard notation in tokamaks (I_p, I_v, I_a, R). Tables 1–3 give a short description of all physical variables and constants used throughout this paper. By taking the derivative of equation (1), this set of equations can be written in matrix form

$$M_2 \dot{x}_p + \Omega_2 x_p = \begin{bmatrix} L_a & M_{av} & M'_{az} \\ M_{av} & L_v & M'_{vz} \\ M'_{az} & M'_{vz} & \alpha \end{bmatrix} \dot{x}_p + \begin{bmatrix} \Omega_a & 0 & 0 \\ 0 & \Omega_v & 0 \\ 0 & 0 & 0 \end{bmatrix} x_p = v_p, \tag{4}$$

where

$$x_p = \begin{bmatrix} I_a \\ I_v \\ zI_{p_0} \end{bmatrix} \qquad \text{and} \qquad v_p = \begin{bmatrix} V_a \\ 0 \\ 0 \end{bmatrix} \tag{5}$$

denote the physical state variables and the input voltage, respectively. This leads to the ODE system

$$\dot{x}_p = -M_2^{-1} \Omega_2 x_p + M_2^{-1} v_p = A_{2_p} x_p + b_{2_p} V_a = A_{2_p} x_p + b_{2_p} u_p. \tag{6}$$

The linearized variations in the tokamak outputs are the quantities, like the fields and fluxes, measured by diagnostic probes (about 100 sensors is typical) and are linear combinations of the linearized state variables, all of which are current sources, i.e.

$$y_p = C_2 x_p. \tag{7}$$

Table 2. The parameters of mutual inductance matrix M and resistance matrix Ω.

Ω_a, Ω_v	Resistances of active coils and vessel eigenmodes (diagonal matrices)
L_a, L_v	Self and mutual inductances of active coils and vessel eigenmodes
M_{av}	Mutual inductances between active coils and vessel eigenmodes
Ω_p	Plasma resistance
L_p	Plasma self-inductance
M_{ap}, M_{vp}	Mutual inductances between plasma and active coils or vessel eigenmodes
M'_{aR}, M'_{vR}, M'_{pR}	Coupling coefficient between radial position and active coils, vessel eigenmodes or plasma
M'_{az}, M'_{vz}, M'_{pz}	Coupling coefficient between vertical position and active coils, vessel eigenmodes or plasma ($M'_{pz} = 0$, [8])
M'_{Rz}	Coupling coefficient between radial position and vertical position
β	The self-coupling coefficient of radial position (see [7,8])
α	The field curvature: self-coupling coefficient of vertical position

Table 3. The plasma and magnetic field parameters at equilibrium.

I_{p0}	Plasma current at equilibrium
R_0	Radial plasma position at equilibrium
n	Decay index $n = -(R_0/B_z)(\partial B_z/\partial R)$, where B_z is the vertical Field at R_0
Γ	Shafranov coefficient

Normally, the locally linearized tokamak model has a wide range of validity, although adding saturating iron to the magnetic circuit can strongly reduce this range of validity.

The dynamical behaviour of system (6) is given by the eigenvalues of the matrix A_{2_p} which are the poles (eigenmodes) of the open-loop system. The non-zero real eigenvalues are given by [12]

$$\lambda_{1,2} = \frac{1}{2}\frac{N \mp \sqrt{N^2 - 4\Omega_a\Omega_v\alpha D}}{D}, \tag{8}$$

where

$$N = -\alpha(L_a\Omega_v + L_v\Omega_a) + M'^2_{vz}\Omega_a + M'^2_{az}\Omega_v \tag{9}$$

$$D = 2M_{av}M'_{az}M'_{vz} - L_aM'^2_{vz} - L_vM'^2_{az} + \alpha(L_aL_v - M^2_{av}). \tag{10}$$

When we consider an elongated plasma, then the PF curvature, α, is positive. For $0 < \alpha < \alpha_c$, where

$$\alpha_c = \frac{L_aM'^2_{vz} + L_vM'^2_{az} - 2M_{av}M'_{az}M'_{vz}}{L_aL_v - M^2_{av}} > 0 \tag{11}$$

is the critical value of α, one eigenvalue is positive corresponding to the unstable characteristic of an elongated plasma. This linear model is not valid in the range $\alpha > \alpha_c$ due to the fact that the plasma mass has been neglected [3].

If we consider the system (6) with zero input voltage ($V_a = 0$) then the time evolution of this system is given by

$$I_a(t) = \varrho_{11}e^{\lambda_1 t} + \varrho_{12}e^{\lambda_2 t}, \tag{12}$$

$$I_v(t) = \varrho_{21}e^{\lambda_1 t} + \varrho_{22}e^{\lambda_2 t},$$

where ϱ_{ij} are real. Since any output $y_p = [y_1 \quad y_2 \quad \dots \quad y_{m_p}]^{\mathrm{T}} = C_2x_p$ is a linear combination of the states it must also evolve as

$$y_k = \rho_{k1}e^{\lambda_1 t} + \rho_{k2}e^{\lambda_2 t}. \tag{13}$$

Due to the unstable pole ($\lambda_1 > 0$), all outputs, including the vertical plasma position zI_p, evolve approximatively as $e^{\lambda_1 t}$, while the second term with $e^{\lambda_2 t}$ can be progressively neglected since $\lambda_2 < 0$ implies that it decays with time.

The instability due to the elongation is usually referred to as 'the vertical position instability'. This denomination is somewhat confusing because it suggests that the vertical position itself is unstable. But all physical states x_p and outputs y_p are generally 'unstable' since they all contain the unstable mode. The term 'vertical instability' is therefore useful jargon rather than mathematically meaningful. It has its legitimacy only in the sense that the unstable mode appears if the algebraic equation defining the vertical plasma position, equation (1), is added to the model.

2.2. *RZIP model*

The RZIP model [7, 8] has a similar structure to the simple second order model. The major difference is in the following three improvements.

(i) The plasma current variation is no longer neglected and the plasma current denoted by I_p is added to the state variable vector. The plasma current circuit has similar properties to a coil circuit and therefore possesses a self-inductance, mutual inductances, coupling coefficients and an ohmic resistance.

(ii) An instantaneous radial force-balance equation is added. Similar to the vertical force-balance it is an algebraic constraint for which a pseudo state variable RI_{p_0} denoting the radial plasma position is introduced into the model.

(iii) The number of active coil currents and vessel eigenmodes is unlimited. The variable $I_a \in \mathbb{R}^{n_a}$ becomes a vector for which each of the n_a elements is the current in a single coil or a structure of coils connected in series. This implies that the voltage input variable denoted by V_a is now also a vector with n_a corresponding voltage inputs. Similarly, $I_v \in \mathbb{R}^{n_v}$ is a vector with n_v different vessel eigenmodes.

These enhancements resulted in the RZIP model with similar notation [8], in which many elements are themselves matrices

$$M\dot{x}_p + \Omega x_p = \begin{bmatrix} L_a & M_{av} & M_{ap} & M'_{aR} & M'_{az} \\ M_{av} & L_v & M_{vp} & M'_{vR} & M'_{vz} \\ M_{ap} & M_{vp} & L_p & M'_{pR} & M'_{pz} \\ M'_{aR} & M'_{vR} & M'_{pR} & \beta & M'_{Rz} \\ M'_{az} & M'_{vz} & M'_{pz} & M'_{Rz} & \alpha \end{bmatrix} \dot{x}_p + \begin{bmatrix} \Omega_a & 0 & 0 & 0 & 0 \\ 0 & \Omega_v & 0 & 0 & 0 \\ 0 & 0 & \Omega_p & 0 & 0 \\ 0 & 0 & 0 & 0 & 0 \\ 0 & 0 & 0 & 0 & 0 \end{bmatrix} x_p = v_p, \tag{14}$$

where

$$x_p = \begin{bmatrix} I_a \\ I_v \\ I_p \\ RI_{p_0} \\ zI_{p_0} \end{bmatrix} \quad \text{and} \quad v_p = \begin{bmatrix} V_a \\ 0 \\ 0 \\ 0 \\ 0 \end{bmatrix}, \tag{15}$$

leading to similar ODEs in the state-space form

$$\dot{x}_p = -M^{-1}\Omega x_p + M^{-1}v_p = A_p x_p + B_p V_a = A_p x_p + B_p u_p. \tag{16}$$

As in the case of the simple second order model, the outputs are linear combinations of the state variables.

$$y_p = C_p x_p. \tag{17}$$

The existence of the instability of the RZIP model again depends on the value of the field curvature α. Due to the structure of the model there exists at most one unstable mode when the plasma is elongated, i.e. $\alpha > 0$. This behaviour of the RZIP model was verified by numerical examples without exception and explained graphically. In [12] the principal ideas and the required assumptions for demonstrating the existence of a single unstable pole for elongated plasmas are laid out.

2.3. CREATE-L model

Contrary to the RZIP model, the CREATE-L model [13] treats plasma deformation by conserving an equilibrium of the plasma current distribution. In addition, the effect of changes to β_p and l_i is evaluated consistently. The explicit constraint equations (algebraic equations expressing zI_{p_0} and RI_{p_0} as a function of the currents in the RZIP model) are eliminated, but retaining force balance, and the model is expressed similarly to the RZIP. Again, the CREATE-L model always has a single unstable mode.

2.4. Implementing ELM-like disturbances in the models

We extend the model defined by equations (16) and (17) by introducing a disturbance input $w = [\Delta\beta_p \quad \Delta l_i]^{\mathrm{T}}$ into the state and the output equations resulting in [13]

$$\dot{x}_p = A_p x_p + B_p u_p + E_p \dot{w}, \tag{18}$$

$$y_p = C_p x_p + F_p w. \tag{19}$$

The three most important disturbance types considered for the ITER design are [1] the following.

- A minor plasma current disruption (MD): this is a sudden drop of both β_p and l_i followed by a slow recovery.
- Compound edge localized mode (CELM): this is similar to the MD but with a smaller amplitude and a faster recovery.
- Type I edge localized modes (ELM1): this is a drop of β_p followed by recovery. The amplitude is similar to that of the CELM, while the recovery time is shorter than for the CELM.

For the analysis, we model a simplified ELM-like disturbance, in which the drop and the recovery are represented as ramps (figures 1(*a*) and (*b*)). In practice, the amplitude, the duration of a disturbance and the time lapses between two disturbances vary strongly from discharge to discharge. Furthermore, the representation of the disturbance by ramps is only an approximation compared with real ELM disturbances. However, since the tokamak system integrates this time-history of the disturbance derivative, we are essentially neglecting the highest frequencies by making this triangular approximation, which is the standard model used during the ITER plasma control design. The longer timescale behaviour will therefore be similar to that of a more structured disturbance.

3. Control strategy

Our proposed control strategy relies on the fact that the current, shape and position controller is split into two parts: (i) a slow controller which is responsible for the plasma current and shape control (the SC controller) and (ii) a fast controller which is responsible for the vertical plasma position stabilization (the VC controller). Although the terminology varies from one

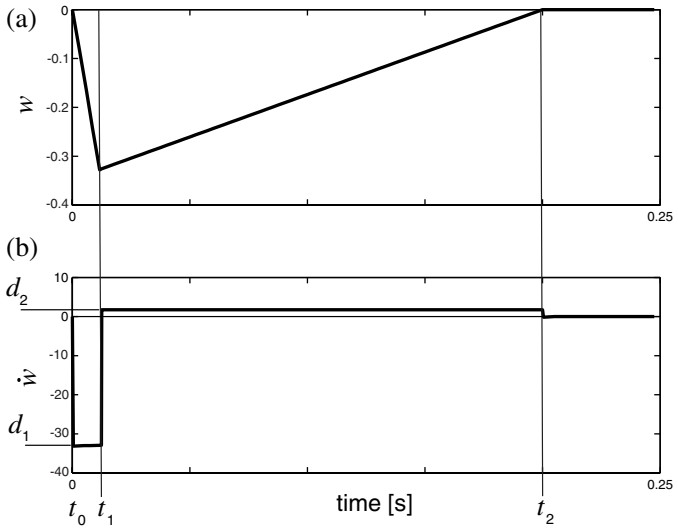

Figure 1. Evolution of an ELM-like disturbance w (*a*) and its derivative $\dot{w}$ (*b*).

tokamak to another, this property is common to ITER, JET, MAST and TCV. In addition, we assume that only one power supply is devoted to the vertical stabilizing control part since our studies on system stability with saturated inputs are limited, so far, to single saturated input systems. Many tokamaks, such as ITER, JET, TCV and AUG, meet these requirements. We assume that the normally slower power supplies on the other PF coil are not reacting strongly to fast disturbances.

This section describes the tokamak closed-loop system for the controller design and is valid for any tokamak meeting these requirements. A full description of the derivation of the equivalent system to be controlled is presented in appendix A. The procedure consists of the following steps:

- incorporating the SC controller into the tokamak model by assuming that it does not saturate the power supplies, and therefore remains linear;
- checking that the SC controller has not introduced an additional unstable mode, an important but frequently overlooked requirement;
- transforming this system into a normalized orthogonal system

$$\dot{x} = Ax + bu + E\dot{w}, \tag{20}$$

where $u \in \mathbb{R}$ is the single normalized input controlled by the VC controller. This system can be subdivided into two independent subsystems, i.e. [15]

$$\begin{bmatrix} \dot{x}_1 \\ \dot{x}_{\mathrm{st}} \end{bmatrix} = \begin{bmatrix} \lambda_1 & 0 \\ 0 & A_{\mathrm{st}} \end{bmatrix} \begin{bmatrix} x_1 \\ x_{\mathrm{st}} \end{bmatrix} + \begin{bmatrix} \lambda_1 \\ b_{\mathrm{st}} \end{bmatrix} u + \begin{bmatrix} E_1 \\ E_{\mathrm{st}} \end{bmatrix} \dot{w}, \tag{21}$$

where $x_1 \in \mathbb{R}$, λ_1 and E_1 describe the unstable subsystem, $x_{\mathrm{st}} = [x_2 x_3 \ldots x_n]^{\mathrm{T}} \in \mathbb{R}^{n-1}$, A_{st}, b_{st} and E_{st} describe the stable subsystem. The output of this normalized system is

$$y_p = Cx + Fw; \tag{22}$$

- transforming the input–output VC controller into a state feedback controller, i.e.

$$\tilde{u} = fx + f_w w; \tag{23}$$

- replacing the VC power supply saturation by the normalized saturation function

$$u = \mathrm{sat}(\tilde{u}) = \begin{cases} -1 & \text{if } \tilde{u} < -1, \\ \tilde{u} & \text{if } -1 \leqslant \tilde{u} \leqslant 1, \\ 1 & \text{if } \tilde{u} > 1. \end{cases} \tag{24}$$

3.1. Input–output controllers compared with state feedback controllers

We consider a general single input-single output system expressed in state-space notation

$$\begin{aligned} \dot{x} &= Ax + bu, \\ y &= cx \end{aligned} \tag{25}$$

and a PD feedback controller which feeds back on a directly measured output of the system being controlled, referred to as an input–output controller:

$$u = k_p y + k_d \dot{y} = k_p cx + k_d c(Ax + bu), \tag{26}$$

leading to

$$u = \left[\frac{1}{1 - k_d cb} (k_p c + k_d cA) \right] x = fx. \tag{27}$$

Since the input u is only a function of x it is evident that any PD controller can be transformed into a state feedback controller, i.e. $u = fx$. On the other hand, the transformation of an arbitrary state feedback controller into a PD controller is only generally feasible for a second order open-loop system. For a higher order system there is not necessarily a similar transformation. This is most easily seen from the fact that the PD controller can only feed back the state in a two-dimensional subspace while the pure state feedback

$$u = fx = [f_1 \quad f_2 \quad \ldots \quad f_n]x$$

can handle the whole space $\mathbb{R}^n$. Since the state feedback controller has more degrees of freedom it allows improved controller design methods and specifically allows us to place all the poles of the closed loop system, in principle. In spite of this clear advantage, tokamaks have not regularly been operated with state feedback control. The primary reason is that we need to create an estimator of all the states, a point to which we shall return in section 5. The representation of real properties of the closed feedback loops, such as delays, is represented in the same way as in the Laplace representation, by a filter. To represent an integral term in a PID feedback loop, an additional state is created, of which the error is the derivative. Equation (25) then increases its order by one for each integral term added.

3.2. The problem of power supply saturation

A change of the vertical plasma position induces a current in the vacuum vessel which provides the required restoring radial field to stop the movement. But due to the resistance of the vacuum vessel, the vessel current and therefore the restoring radial magnetic field decay rapidly. It is therefore indispensable to provide an additional radial field which is supplied by actively powered coils. Voltage saturation of the power supplies limits the rate of change of the magnetic field. For small disturbances, the displacement of the vertical plasma position and the destabilizing magnetic force are small. To bring the plasma back to its nominal equilibrium position, a small rate of change of the magnetic field, providing the necessary amount of radial field within a reasonable time lapse, is sufficient and thus the power supplies do not saturate. For larger disturbances the rate of change of the field has to be larger, and the power supplies

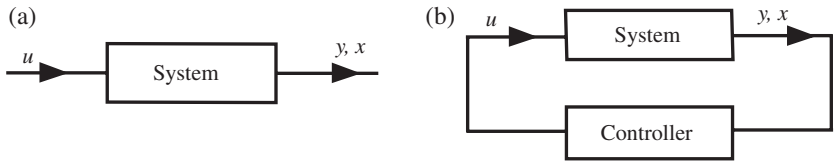

Figure 2. (*a*) Pure open-loop system, (*b*) closed-loop system with controller.

may saturate. In this case, the rate of change of the field reaches its limit and no longer compensates the decaying passive structure currents, which leads to an inevitable loss of control. Once voltage saturation is reached, we are sure to deliver the maximum available rate of change of the magnetic field, and there is no way to do better for the given power supply.

The work presented by Scibile [16, 17] illustrates this point very well. A sliding mode bang–bang controller with a single power supply was proposed for JET based on a linear second order model. One of its demonstrated properties was to ensure the maximum reachable stability performance under voltage saturation.

However, a bang–bang controller has one important drawback which is linked to the minimization of ac losses in superconducting coils [18, 12]. The main result of this earlier ac losses analysis revealed that to reduce the ac losses we need to design a controller which generates a non-oscillating, low amplitude and low frequency control voltage signal. A sliding mode bang–bang controller does just the contrary: it generates a non-smooth signal with a maximum amplitude and an oscillating signal with high frequencies during sliding mode. Therefore, such a controller has never been considered for tokamaks with superconducting coils.

Another drawback illustrated by the sliding mode controller is the fact that considerable knowledge is required when designing and implementing such a control algorithm. This is another reason why most controllers implemented for tokamaks are still PID controllers.

Finally, the application of the particular sliding mode bang–bang controller requires a linear second order model, while in general the linear models derived from RZIP and CREATE-L are of orders of 50–100, as discussed in section 2.

3.3. Stability notions

For stability analysis in state-space we first need to introduce two formal stability notions. We consider an arbitrary dynamical system and an arbitrary controller.

First, we recall the notion of the null controllable region (NCR) considered for open-loop systems as depicted in figure 2(*a*).

Definition 1. *Let* $\Phi(t, x_0, u(t))$ *denote the state of a dynamical system at time* $t > 0$*, starting with the initial condition* x_0 *at* $t = 0$ *and subjected to the input* $u(t)$*. A state* x *is said to be null controllable if there exists an admissible control* $u(t)$ *that steers the trajectory* Φ *to the origin, i.e.*

$$\lim_{t\to\infty} \Phi(t, x, u(t)) = 0.$$

All states being null controllable belong to the set of the NCR which is denoted by $\mathcal{C}$*. The boundary of* $\mathcal{C}$ *is referred to as* $\partial\mathcal{C}$*.*

The second stability notion is the region of attraction (RoA) linked to closed-loop systems with a controller as depicted in figure 2(*b*).

Definition 2. *Let $\Phi(t, x_0)$ denote the state of a closed-loop system at time t, starting with the initial condition x_0 at $t = 0$. The RoA $\mathcal{A}$ is the maximum region in state-space for which the state of the closed-loop system asymptotically reaches the origin, i.e.*

$$\mathcal{A} = \left\{x \in \mathbb{R}^n : \lim_{t\to\infty} \Phi(t, x) = 0\right\}.$$

The boundary of $\mathcal{A}$ is denoted by $\partial\mathcal{A}$.

Definitions 1 and 2 imply that the RoA is always smaller or equal to the NCR, i.e. $\mathcal{A} \subseteq \mathcal{C}$. The NCR can be interpreted as the maximal RoA that can be obtained with any controller, i.e. there exists no controller for which the resulting RoA is larger than the NCR. The corollary is that no controller can be more stabilizing than a controller whose RoA is equal to the NCR. Our challenge now formally becomes one of finding the latter controller.

3.4. NCR and RoA for a tokamak-like dynamical system

In what follows we analyse the dynamics of system (20) with the orthogonal matrix A. Furthermore, we do not take into consid0eration the disturbance (i.e. $w = 0$), which will be discussed in section 4. Therefore, we consider the open-loop system

$$\dot{x} = Ax + bu. \tag{28}$$

For a system with a normalized saturated input defined by equation (24), the set of admissible control is given by $u(t) \in [-1, 1]$.

3.4.1. The shape of the NCR. Consider system (28) with saturated input,

$$\dot{x} = Ax + b\ \mathrm{sat}(\tilde{u}). \tag{29}$$

Its NCR is given by ([15, 16, 19, 20])

$$\mathcal{C} = \{x \in \mathbb{R}^n : |x_1| < 1\} \qquad \text{and its boundaries are defined by} \tag{30}$$

$$\partial\mathcal{C}_+ = \{x \in \mathbb{R}^n : x_1 = 1\}, \qquad \partial\mathcal{C}_- = \{x \in \mathbb{R}^n : x_1 = -1\}. \tag{31}$$

Consider the unstable part of system (28), which is $\dot{x}_1 = \lambda_1 x_1 + \lambda_1 u$. If we want to steer the unstable state to the origin from an initial condition $x_1 > 0$, then we need to obtain $\dot{x}_1 < 0$. For $x_1 \geqslant 1$ we have

$$\dot{x}_1 = \lambda_1(x_1 + u) \geqslant 0$$

for $u \in [-1, 1]$, which means that the unstable state x_1 cannot be steered back to the origin. On the other hand, for all $0 < x_1 < 1$ there always is a value of $u \in [-1, 1]$ for which

$$\dot{x}_1 = \lambda_1(x_1 + u) < 0.$$

This means that there is always a saturated input which can drive the unstable state back to the origin. A similar argument treats $x_1 < -1$. Once the unstable state reaches $x_1 = 0$ by a suitable input, then the input can be set to zero ($u = 0$) and the stable states $x_{\mathrm{st}} \in \mathbb{R}^{n-1}$ of the stable part of system (28) asymptotically reach $x_{\mathrm{st}} = 0$, since all eigenvalues of A_{st} are negative. From this straightforward argument, we deduce that the boundaries of the NCR are only due to the fact that system (29) possesses an unstable state x_1. The NCR is therefore only bounded in one dimension of $\mathbb{R}^n$ along x_1.

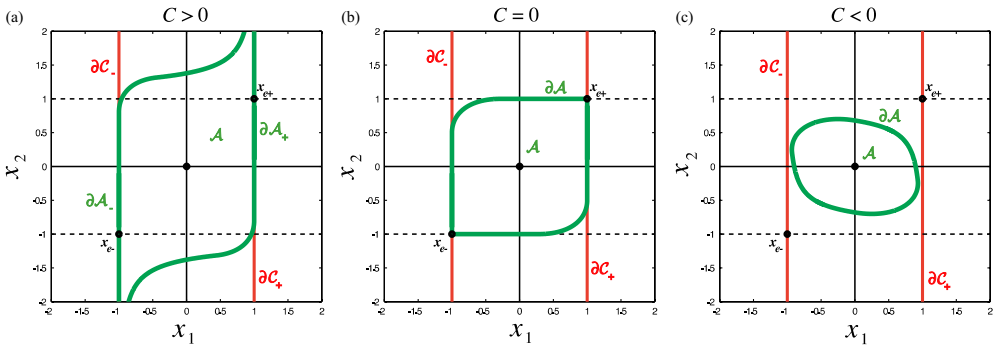

Figure 3. The RoA (green) and NCR (red) for a second order system. There exist different shapes of the RoA as a function of the system and controller parameters $C = C(\lambda_1, \lambda_2, f_1, f_2)$. (*a*) Hyperbolic shape. (*b*) Heteroclinic connections. (*c*) Limit cycle.

3.4.2. The shape of the RoA. To determine the RoA we consider the linear state feedback controller

$$\tilde{u} = fx = f_1x_1 + f_2x_2 + f_3x_3 + \cdots + f_nx_n. \tag{32}$$

The resulting closed-loop system is given by

$$\dot{x} = Ax + b\,\mathrm{sat}(fx). \tag{33}$$

Our first approach was to start with the simple second order system with one stable and one unstable pole, where the goal was to understand the fundamental nature of the problem linked to the characterization of the RoA.

For this class of systems, it is possible to determine a scalar condition, referred to as C, which is an analytical function of the system parameters λ_1 and λ_2 and the controller parameters f_1 and f_2, i.e. $C(\lambda_1, \lambda_2, f_1, f_2) : \mathbb{R}^4 \to \mathbb{R}$.

Figure 3 shows the different shapes of the RoA (solid green) and the boundaries of the NCR (solid red) for the second order system. The sign of the analytical condition C gives information on the type of the RoA:

- $C > 0$: unbounded hyperbolically shaped;
- $C < 0$: bounded by a limit cycle;
- $C = 0$: the limit case between the two previous types of RoA corresponds to a set bounded by two heteroclinic connections.

The exact description of the analytical condition C and the complete proofs of the analysis of the RoA for second order systems are given in [12].

Our hope was to apply this understanding in a similar way to higher order systems, but still with a single unstable pole. However it turned out that the analysis of the second order system itself was not as simple as it appeared. Nevertheless, the problem could be completely solved by applying

- results about equilibrium points and the RoA given in [19];
- the fundamental theorems from Poincaré and Bendixson, which give results on the existence of limit cycles for a second order system;
- some results from the contraction analysis of second order systems, where one part is provided by [15], and the other part is a new contribution presented in [12].

There is no way to apply these results for second order systems to higher order systems, since the analysis relies on methodologies like the Poincaré and Bendixson theorems which are only valid for second order systems. Thus, since the work for second order systems was not at all trivial, the search for characterizing the RoA for higher order systems had to be abandoned. Note that other researchers also tried to obtain results for higher order systems without success [15]. We therefore conclude that the identification of the RoA by means of conservative methods like Lyapunov function analysis remains state-of-the-art for higher order systems.

3.5. Enlarging the RoA

3.5.1. The global stability. From this somewhat disappointing result a new idea arose. Is there a possibility of slightly modifying an existing linear controller to derive a new controller for which its RoA is equivalent to the NCR? Designing a controller whose RoA is equal to the NCR is an essential step since it produces the following two major advantages.

- Since the NCR is the maximum possible RoA, there exists no controller for which the resulting closed-loop system possesses a larger RoA than the NCR (section 3.3). Thus, if the RoA is equal to the NCR, we can state that, as far as the stability region is concerned, we can do no better. We call such a controller a globally stabilizing controller.
- The exact determination of the NCR and consequently of the RoA is very simple. We have shown in section 3.4 that its boundaries are only due to the unstable state, while the stable states are unbounded in state-space. Thus, by only knowing the value of the unstable state we can determine whether the state of the tokamak in operation is inside or outside the RoA. This will allow us to detect a loss of control.

We first show that there exists a linear state feedback controller for which the RoA is equal to the NCR ($\mathcal{A} = \mathcal{C}$) [19]. We consider the linear state feedback control (32) which stabilizes system (28). A globally stabilizing controller, i.e. $\mathcal{A} = \mathcal{C}$, is obtained if and only if $f_2 = f_3 = \cdots = f_n = 0$, i.e.

$$\tilde{u}(x) = f_1 x_1. \tag{34}$$

The unstable subsystem then becomes

$$\dot{x}_1 = \lambda_1(x_1 + \mathrm{sat}(\tilde{u})) = \lambda_1(x_1 + \mathrm{sat}(f_1 x_1)).$$

Since the stabilization of system (28) requires $1 + f_1 < 0$, then for all $x \in \mathcal{C}$, i.e. $|x_1| < 1$, the unstable state x_1 converges to zero independently of the other stable states. The stable subsystem becomes $\dot{x}_{\mathrm{st}} = A_{\mathrm{st}} x_{\mathrm{st}}$ and since A_{st} is stable, all stable states converge to the origin, i.e. $x_{\mathrm{st}} \to 0$, but are not controlled.

For all other linear controllers in which at least one of the gains $f_2, f_3, \ldots, f_n$ is non-zero, the RoA is always smaller than the NCR ($\mathcal{A} \subset \mathcal{C}$). This is explained in detail in [12].

An intuitive insight into these results on global stability can be provided by analysing the RoA of a second order system. Figure 4 depicts the variation of the RoA as a function of the controller gain f_2. For highly negative values of f_2 the boundary of the RoA is a limit cycle. By increasing the value of f_2 the shape of the RoA becomes hyperbolical. For positive values of f_2 the shape is hyperbolic too, but mirror-inverted. Our specific case of $f_2 = 0$ is the only one for which the RoA is equal to the NCR, which is our aim.

3.5.2. The performance. The particular controller (34) has the feature of global stabilization, but suffers from the fact that only one eigenvalue of the closed-loop dynamics can be influenced. Actually, since the $n - 1$ controller gains $f_2, f_3, \ldots, f_n$ have to be zero, only the controller

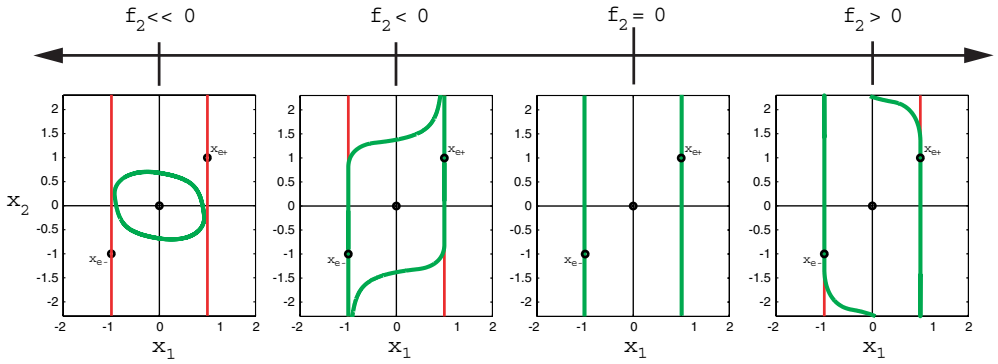

Figure 4. The variation of the RoA as a function of the controller parameter f_2: green—RoA; red—NCR.

gain f_1 can be tuned. Thus, only the unstable pole can be tuned, while all the other eigenvalues stay at the values of the stable subsystem. This obviously limits the effect of the controller on the full performance, since we cannot set the controller parameters $f_2,\ f_3, \ldots, f_n$ to zero and achieve the desired performance. There are many performance requirements one might impose on a controller. We consider the fast rejection of disturbances as the most essential performance indicator. For ITER, this means that the vertical position will be stabilized but the plasma-wall gaps and divertor strike-points are no longer controlled!

There is therefore a tradeoff between global stability and performance. For some controllers, we are not always able to satisfy the required performance over the whole RoA. We therefore define the notion of local performance where we guarantee the performance locally around the equilibrium point (the origin of the linearized model). This means that for small enough disturbances the required performance is guaranteed, while for large disturbances some controllers may lose the required performance for the sake of guaranteeing global stability.

3.5.3. The reduction of ac losses. Minimizing ac losses is an additional performance requirement for tokamaks with superconducting coils. A detailed discussion concerning the reduction of the ac losses is presented in [18, 12]. The main goal for reducing ac losses is to design controllers which generate control signals with the smallest possible oscillations, with both amplitudes as small as possible and frequencies as low as possible.

3.5.4. Standard controllers. In the literature we find various standard controllers which possess the following global stabilizing property:

(i) *Controller switching* from the global stabilizing controller (i) $\tilde{u} = f_1 x_1$ to the full parameter controller (ii) $\tilde{u} = fx$ achieving the desired performance [15, 20]: when the unstable state is near the boundary of the NCR the controller (i) is used to ensure the global stability. Once the unstable state is close to the origin the controller (ii) is used to achieve the desired performance. This allows us to simultaneously ensure global stability and local performance. The problem is that switching from one controller to another implies a discontinuity and may give rise to oscillations in the control signal.

(ii) *Time optimal controller* [21]: this controller belongs to the class of bang–bang controllers, switching the control signal from the maximum value to the minimum value and vice versa. In our case, the maximum and minimum values are given by the saturation levels,

i.e. +1 and −1. The problem linked to the time optimal controller is the fact that in the presence of noise and disturbances a chattering of the control signal is inevitably induced.

(iii) *Near-time optimal VSC controller* [16]: this controller is a sliding-mode bang–bang controller and generates chattering in the control signal during the sliding-mode phase.

Since for all three controllers either oscillations or chattering are generated in the control signal, they are not suited to superconducting tokamak control.

3.5.5. The CNGSC controller. Our principal objective was to propose a new controller which satisfies the three requirements discussed above:

(i) global stability;
(ii) performance;
(iii) reduction of ac losses.

We consider a modified controller

$$\tilde{u}(x) = f_1x_1 + k(x)(f_2x_2 + f_3x_3 + \cdots + f_nx_n) \qquad u = \mathrm{sat}(\tilde{u}), \tag{35}$$

where $f = [f_1 \quad f_2 \quad f_3 \quad \cdots \quad f_n] \in \mathbb{R}^{1\times n}$ and $k(x)$ is a scalar function of the vector x. Assume that f has been designed to deliver the desired performance (requirement (ii) of the closed-loop system near the origin, for small disturbances. If we set $k(x) = 1$, then the controller (35) corresponds to the designed linear state feedback controller with the desired performance. If $k(x) = 0$, then the stable states are not fed back, leading to global stability ($\mathcal{A} = \mathcal{C}$), as shown in section 3.5.1. A nonlinearity is introduced by choosing:

$$k(x) = 1 - |x_1| \tag{36}$$

or

$$k(x) = 1 - x_1^2, \tag{37}$$

where $0 < k(x) \leqslant 1$ since within the NCR $|x_1| < 1$.

The idea behind this nonlinear controller is as follows. If $x_1 \approx 0$, then $k(x) \approx 1$ which implies that the controller is approximately the full linear state feedback $\tilde{u} \approx fx$. In this case, the controller concentrates on local performance (requirement (ii)). If the unstable state approaches the boundary of the NCR $\mathcal{C}$, $x_1 \approx \pm 1$ and $k(x) \approx 0$. This implies that the controller is approximately the linear state feedback $\tilde{u} \approx f_1x_1$, where it focuses on the stabilization of the unstable state and global stability (requirement (i)). Since the controller (35) and (36) is a continuous one, oscillations and chattering are avoided and requirement (iii) is also fulfilled. This new controller can be considered to be continuous nonlinear variation from the full state controller (equation (32)) to the global stabilizing controller (equation (34)) and we therefore refer to it as the CNGSC.

For second order systems an analytic proof of the global stability for slightly more conservative conditions is given in [12, 22]. Slightly more conservative conditions means that we were not able to provide an analytic proof for the whole class of stabilizing controllers but only for a large subset of this class. Nevertheless, all results obtained from simulations seem to reveal global stability for the whole class. For higher order systems the quest for an analytic proof of the global stability was highly complicated and so far unsuccessful. Therefore, the demonstration of the global stability of higher order systems is only based on numerical results by means of simulation.

4. Simulation by means of linear models

4.1. Validation on ITER with the linear CREATE-L response model

In this section we validate the method on ITER simulations using its linear CREATE-L plasma response model [14]. We use the SC and VC input–output feedback controllers previously proposed [23] in which the SC controller design neglects the currents induced in the passive structure, but includes weak integral gain. The aim is to compare, in simulations, the reference VC feedback controller with our proposed CNGSC feedback controller. The reference VC controller, expressed as a state feedback controller, is given by equation (23), i.e.

$$\tilde{u} = [f_x\, f_w]\begin{bmatrix} x \\ w \end{bmatrix} = f_1 x_1 + f_2 x_2 + f_3 x_3 + \cdots + f_n x_n + f_w w,$$

where f_w expresses the disturbance feedback gain. The CNGSC controller is given by applying equation (35), i.e.

$$\tilde{u} = f_1 x_1 + k(x)(f_2 x_2 + f_3 x_3 + \cdots + f_n x_n + f_w w),$$

where the disturbance input w is handled just like the stable states. For the nonlinear function $k(x)$ we use the smooth square function (equation (37)). This nonlinearity is solely valid inside the NCR ($|x_1| \leqslant 1$). In this section we will find that the trajectory of the closed-loop system may leave and reenter the NCR during a disturbance. We therefore define the nonlinear function to be zero outside the NCR ($|x_1| > 1$) by adding the following extension:

$$k(x) = \begin{cases} 1 - {x_1}^2 & \text{if } |x_1| \leqslant 1, \\ 0 & \text{if } |x_1| > 1. \end{cases}$$

The comparison of the reference controller with the CNGSC controller is illustrated in simplified phase diagrams. Since we are dealing with a high order system (50–100 states) we cannot show the evolution of all the states. Thus, the planar phase diagrams can only show the evolution of two states: (i) the unstable state, referred to as x_1 and (ii) one of the most disturbed stable states, referred to as x_s. We recall that x_1 is the only unstable state and that all other states are therefore stable. The state x_s is simply one of the many orthogonal states and has no physical meaning other than this. Indeed, we searched desperately for a physical significance of x_1 itself, and found none, other than the fact that it is that orthogonal state (a specific linear combination of the physically significant states from which we constructed our original model) which grows exponentially when the feedback loop is broken. Since all other states are stable, such as x_s, they remain bounded in the absence of feedback control. They are not, in the strict sense, controlled in that their values are not being determined with respect to a reference value, but simply remain bounded. There is no link between these states and the physical description of the plasma, such as its shape. The states each contain the details of the passive conductors, the details of the active conductors and the distribution of the plasma current. In what follows, the RoA of the reference controller is referred to as $\mathcal{A}_r$ and the RoA of the CNGSC controller is referred to as $\mathcal{A}_c$. We show in the simulations that the RoA for the reference controller is strictly a subset of the NCR $\mathcal{A}_r \subset \mathcal{C}$. Furthermore, we show that the trajectories of the closed-loop system with the CNGSC controller converge to the origin if the initial conditions are inside $\mathcal{A}_c = \mathcal{C}$.

4.1.1. Arbitrary initial conditions. For this first example we do not disturb the system, leaving $\dot{w} = 0$. Instead, we simply set non-zero initial conditions. The phase diagram (figure 5) shows the evolution of x_1 and x_s. The starting point x_{init} denotes the initial conditions which are located inside the NCR $x_{\text{init}} \in \mathcal{C}$. Since for the CNGSC controller the initial conditions are located

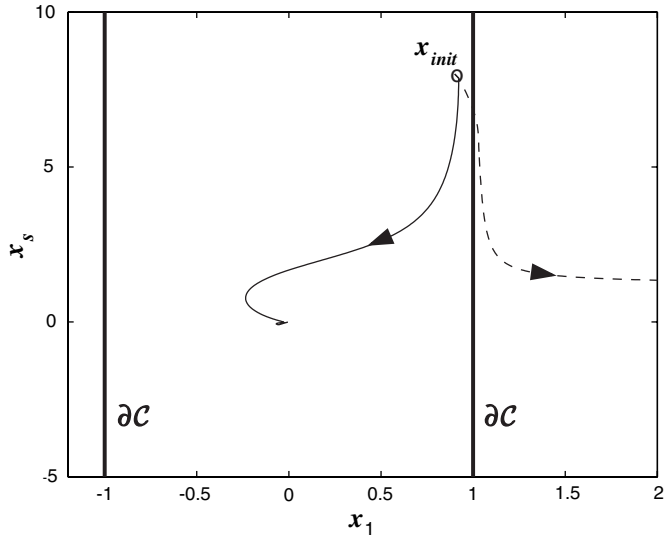

Figure 5. Example with non-zero initial conditions (x_{init}) and without disturbance, dashed: reference controller, solid: CNGSC controller. The model is CREATE-L.

within the RoA ($x_{\text{init}} \in \mathcal{A}_c = \mathcal{C}$) the trajectory converges to the origin. For the reference controller the trajectory diverges, thus confirming by simulation that $\mathcal{A}_r \subset \mathcal{C}$.

4.1.2. Small disturbance. To disturb the system away from the equilibrium we apply an ELM disturbance as illustrated in figure 1 (section 2.4). The disturbance starts at t_0, reaches its maximum at t_1 and vanishes at t_2.

The trajectories are shown in figure 6 for a very small disturbance (dotted lines), in which the responses with the CNGSC and reference controllers are almost indistinguishable. A larger disturbance, stabilized by the reference controller (dashed line), illustrates a superior rejection by the CNGSC controller (solid line) due to the concentration on the unstable state.

At the discontinuities in the disturbance waveform (figure 1), the states respond similarly to positive or negative steps in the waveform derivative, thus provoking an increase in x_1 at t_2, just as we had an increase in x_1 at t_0.

4.1.3. Large disturbance. The evolution of the trajectories for both controllers during and after a large disturbance is illustrated in figure 7. At t_2 the states of the systems with both controllers are in $\mathcal{C}$. Since for the CNGSC controller $\mathcal{A}_c = \mathcal{C}$, the trajectory converges to the origin. For the reference controller the trajectory diverges and thus we conclude that the state is not in $\mathcal{A}_r$ at t_2 and that $\mathcal{A}_r \subset \mathcal{C}$.

4.1.4. Very large disturbance. The third example shows the trajectory evolutions for a much larger disturbance amplitude (figure 8). Both trajectories leave the NCR $\mathcal{C}$ and only the trajectory for the system with the CNGSC controller re-enters $\mathcal{C}$. Therefore, this trajectory converges to the origin and the trajectory of the system with the reference controller diverges. The fact that the trajectory can leave and re-enter the NCR (or the RoA) is due to the disturbance input w. During the disturbances, the controlled system is no longer symmetric and the NCR is displaced to smaller or larger values but recovers when the disturbance finishes. The reason for this is analysed in appendix B.

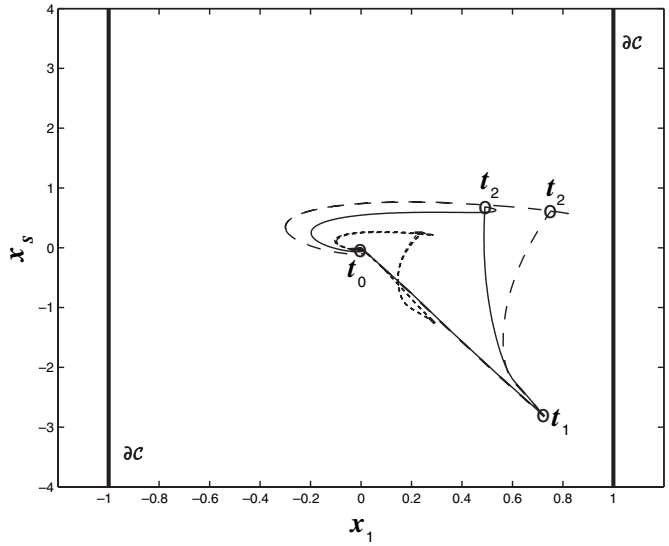

Figure 6. Example with a very small disturbance, dotted: reference and modified controllers are almost indistinguishable. Example with a small disturbance, dashed: reference controller, solid: CNGSC controller.

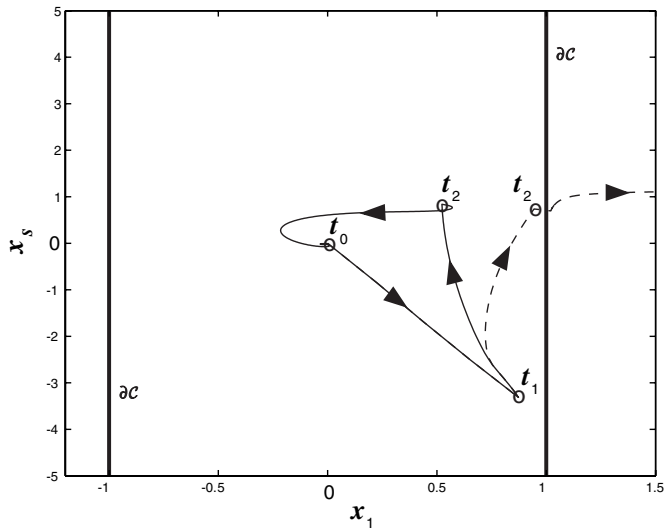

Figure 7. Example with a large disturbance, dashed: reference controller, solid: CNGSC controller.

When the amplitude and the time intervals of the drop and recovery of the disturbance are known, it is theoretically possible to predict from the tokamak model whether the trajectory will be inside or outside the NCR at t_2. In practice, these time intervals are not known beforehand and the shape of a disturbance differs from the simplified ELM-like model proposed in this paper, and the prediction of the location of the trajectory at t_2 may not be accurate enough. Thus, since it is difficult to know whether the state remains in the RoA during the disturbance,

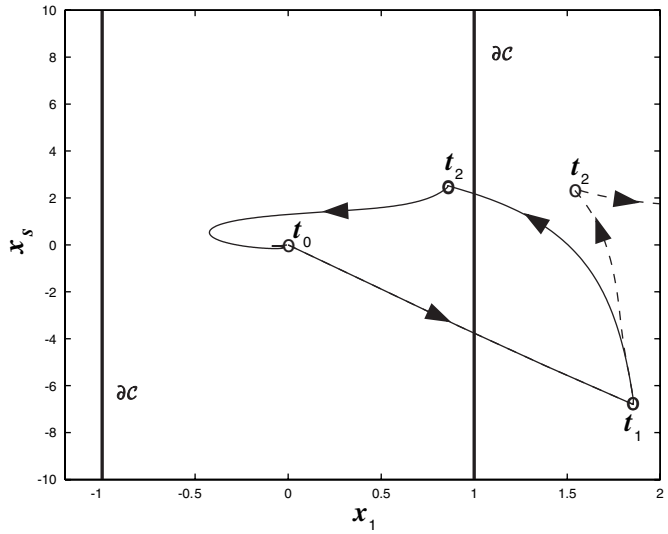

Figure 8. Example with a very large disturbance, dashed: reference controller, solid: CNGSC controller.

we have to wait until the disturbance vanishes at $t = t_2$ to determine if the controller is able to stabilize the system or not.

For the small disturbance, the two controllers are indistinguishable. For the larger disturbances, the unstable state x_1 is brought back to the origin faster when the CNGSC controller is used. This is a strong benefit of the nonlinear function $k(x)$ which helps the controller concentrate on the unstable state in the proximity of the boundaries of the NCR $\mathcal{C}$ and beyond it. For the largest disturbance, the reference controller failed to maintain stability.

4.2. Validation on JET with the linear CREATE-L model

We have implemented the same technique on the CREATE-L model for JET [24], including their reference controller. We increased the amplitude of the disturbance until the closed-loop system with the reference controller loses control due to saturation of the fast radial field amplifier (FRFA) chopper supply. The simulation was repeated with the CNGSC controller and control is no longer lost.

Figure 9 shows an example of the evolution of the vertical plasma position z and the FRFA control voltage for a very large ELM disturbance in JET. The disturbance starts at t_0, reaches a maximum at t_1 and vanishes at t_2 (vertical dashed lines). The reference controller loses stability just after t_1.

5. State and disturbance reconstruction

Up to now, we have assumed that the values of all the state variables x and the disturbance input w are directly accessible, i.e. the state variables and the disturbance input are measurable. But in practice this is never the case for tokamaks. We therefore have to extract an estimate of the state, referred to as $\breve{x}$, as well as the disturbance, referred to as $\breve{w}$, by means of the measurable outputs which are principally the magnetic diagnostic measurements. For controller analysis and design purposes, we consider an ideal reconstruction procedure and

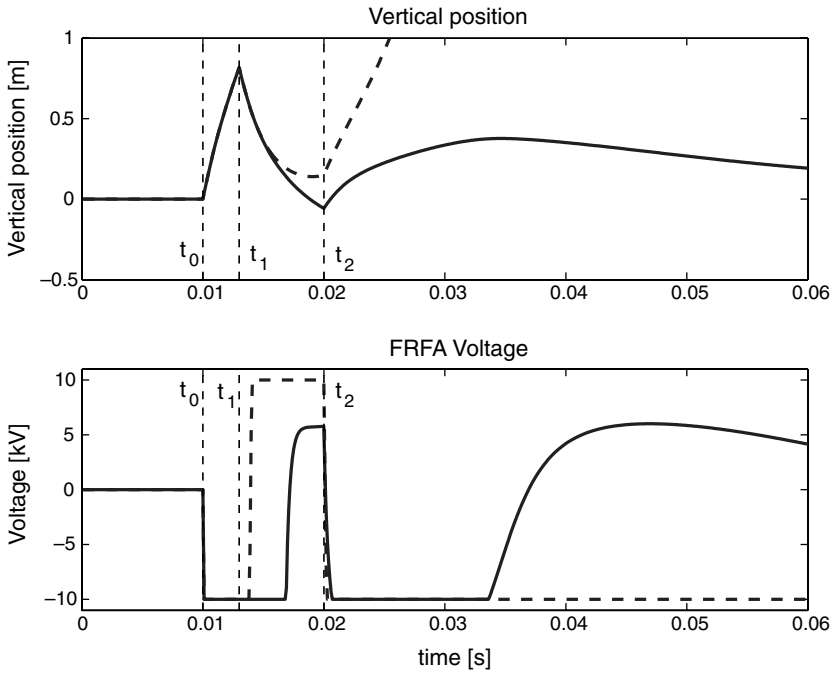

Figure 9. The CNGSC controller (——) on a JET simulation. The reference controller (- - - -) loses control. The model is CREATE-L. The FRFA voltage is the feedback controller demand voltage, not the chopper power supply output.

assume that the reconstructed state $\breve{x}$ and disturbance $\breve{w}$ are equivalent to the actual state x and disturbance w.

There are 3 different state vectors in the tokamak closed-loop system (equation (A.5)) which are

$$x_s = \begin{bmatrix} x_p \\ x_{\mathrm{sc}} \\ x_{\mathrm{vc}} \end{bmatrix},$$

where x_p denotes the physical state variables of the linearized tokamak model, x_{sc} the state of the SC controller and x_{vc} the state of the VC controller. Since the SC controller is implemented explicitly in hardware or software, its state x_{sc} is directly accessible. We simply have to implement the input–output VC controller in such a way as to provide direct access to its internal state x_{vc}. The challenge is to reconstruct the linearized tokamak model state x_p. In this section, we propose a fast static reconstruction which relies on the least squares method. Once all states are reconstructed, the reconstructed normalized state is obtained by means of the linear state transformation (equation (A.8))

$$\breve{x} = T^{-1}\breve{x}_s.$$

We also have to reconstruct the disturbance input w. By considering the linear tokamak model, we can show that the disturbance input w can also be handled as a state [12].

For any state reconstruction, measurable plant outputs have to be available. In the case of the linear tokamak model the output y_p contains two different parts: (i) the direct physical outputs which are the magnetic diagnostic measurements and (ii) derived physical plasma parameters like the vertical position z and the radial position R of the plasma, the gaps g

and the plasma current I_p. These plasma parameters are normally linear combinations of the magnetic diagnostic measurements since it is not yet possible to estimate all the plasma parameters directly in real-time. In what follows, we define the magnetic diagnostic output as

$$y_{\mathrm{md}} = \begin{bmatrix} B_{\mathrm{pol}} \\ \Psi \\ I_{\mathrm{pol}} \end{bmatrix} = [C_{\mathrm{md}} \quad F_{\mathrm{md}}] \begin{bmatrix} x_p \\ w \end{bmatrix} = \begin{bmatrix} C_{B_{\mathrm{pol}}} & F_{B_{\mathrm{pol}}} \\ C_{\Psi} & F_{\Psi} \\ C_{I_{\mathrm{pol}}} & F_{I_{\mathrm{pol}}} \end{bmatrix} \begin{bmatrix} x_p \\ w \end{bmatrix}, \tag{38}$$

where B_{pol} denotes the value of the poloidal magnetic field probes, Ψ that of the poloidal flux loops and I_{pol} the currents in the PF coils.

5.1. Reconstruction with the least squares method

We consider the linear problem (38) for which we seek to solve for $[x_p \quad w]^{\mathrm{T}}$. If we consider the output $y_{\mathrm{md}} \in \mathbb{R}^{m_{\mathrm{md}}}$, the state $x_p \in \mathbb{R}^{n_p}$ and the disturbance input $w \in \mathbb{R}^{l_p}$ then the least squares method can be applied if the condition $m_{\mathrm{md}} > n_p + l_p$ is satisfied, i.e. the number of outputs has to be superior to the total number of state variables and disturbance inputs. This condition fits in general since there are about 100 different magnetic diagnostic measurements, while a typical linear tokamak model possesses about 50 state variables, and the disturbance input is modelled with 2 different inputs. Thus, by applying the least squares method, the state reconstruction is given by taking the pseudo-inverse of the output matrix of equation (38)

$$\begin{bmatrix} \breve{x}_p \\ \breve{w} \end{bmatrix} = [C_{\mathrm{md}} \quad F_{\mathrm{md}}]^{\dagger} y_{\mathrm{md}}. \tag{39}$$

Since the outputs B_{pol} and Ψ have values which are about 10^5 times smaller than I_{pol} the problem is not well conditioned and the computation of the pseudo-inverse matrix can generate severe errors in the state reconstruction estimation. It is therefore important to normalize the matrix $[C_{\mathrm{md}} \quad F_{\mathrm{md}}]$ and the output y_{md} [12].

5.2. Robustness of the reconstruction

Since the proposed least squares reconstruction method relies on the pseudo-inverse of both output matrices of the linearized tokamak model, we assume that the reconstruction is only accurate in the neighbourhood of the linear model's linearization equilibrium. In this section, we present a preliminary study of the robustness of this reconstruction method by analysing the accuracy of the reconstruction when the state of the tokamak plant is steered away from this linearization equilibrium.

We focus on the most important state of the system, the unstable state x_1. Furthermore, we only consider the most important plasma parameter variations occurring during a discharge, restricting ourselves to the analysis of a varying elongation κ, of a varying vertical plasma position z and during the plasma current ramp-up and ramp-down. We additionally consider two similar discharges, where we derive the linear tokamak model by means of one discharge and apply the reconstruction to the other discharge. This allows us to analyse whether the reconstruction method based on one linear tokamak model is robust for similar discharges.

This study was carried out by analysing experimental TCV discharges. The linearized tokamak model was obtained with RZIP. The time at which the linear model was derived from the discharge is defined as the linearization equilibrium time, denoted as t_0. To avoid the reconstruction of the disturbance input w we assume that no important disturbances occur during the discharges considered. The state reconstruction was done with the normalization

reconstruction, where the normalized pseudo-inverse matrix at t_0 is denoted as $C_0^\dagger$. With this, we obtain a simplified state reconstruction given by

$$\breve{x}_p = C_0^\dagger y_{\mathrm{md}}. \tag{40}$$

We assume that in general the SC controller plays only a minor role in the stabilization of the tokamak and only has a limited influence on the unstable state. We therefore neglect the effect of the SC controller on the unstable state but draw attention to the fact that this becomes a constraint on the SC controller design. Furthermore, since the tokamak system and the VC controller are connected in series, from the point of view of the state feedback controller, the state of the tokamak x_p and the state of the VC controller x_{vc} are totally decoupled. Thus, to get an estimate of the normalized system states, only the physical state variables x_p are required, i.e.

$$x = T^{-1}x_p, \qquad A = T^{-1}A_pT \qquad \text{and} \qquad b = T^{-1}B_{p_{\mathrm{vc}}}.$$

With this, the reconstructed value of the unstable state $\breve{x}_1$ can be derived from

$$\breve{x} = T^{-1}\breve{x}_p = T^{-1}C_0^\dagger y_{\mathrm{md}} \tag{41}$$

in which $\breve{x}_1$ is the first state variable of the state vector $\breve{x}$.

For the robustness study the following three TCV discharges were considered, all of which are in limited ohmic L-mode:

- #12868
  With this discharge we analyse the influence of a variation of the elongation κ in the presence of a variation of the plasma current I_p on the state reconstruction. The vertical plasma position is kept approximately constant $z \approx 0.09$ m.
- #24377
  By means of this discharge we analyse the influence of a variation of the plasma vertical position z on the state reconstruction. I_p and κ are kept constant.
- #24375
  This discharge is similar to discharge #24377 except that the plasma vertical position z does not vary. This discharge is used to obtain the linear tokamak model and the resulting state reconstruction matrix $C_0^\dagger$. The state reconstruction is then applied to the similar discharge #24377. This permits us to analyse whether the reconstruction method computed by means of discharge #24375 is accurate enough for the similar discharge #24377.
  Furthermore, this discharge is used to analyse the robustness of the state reconstruction method during the plasma current ramp-up and the ramp-down.

Figure 10 depicts the evolution of the plasma current I_p, the elongation κ and the vertical plasma position z for the three discharges, provided from the plasma equilibrium reconstruction code LIUQE [25].

The analysis of the state reconstruction robustness is done simply by comparison. Thus, the evolution of the reconstructed states has to be compared with the evolution of states which can be considered as a reference. The equilibrium reconstruction codes do not provide the evolution of the unstable state x_1 and we have to provide the unstable state reference evolution in another way.

We apply a piecewise linearization of the discharge by means of the linear RZIP tokamak model. For this purpose we subdivide the duration of a discharge into discrete time intervals, using t_k with $k \in \mathbb{Z}$. At each time step t_k we derive an RZIP model with which we compute the corresponding normalized pseudo-inverse matrix $C_k^\dagger$.

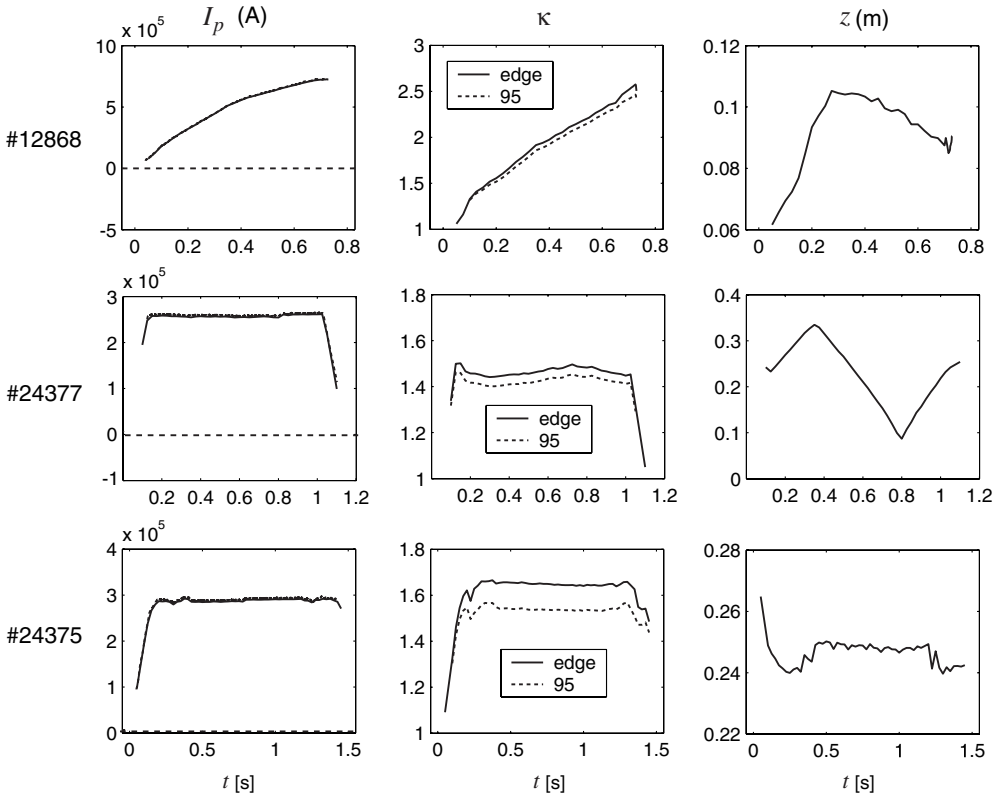

Figure 10. The evolution of the plasma current I_p, the elongation κ and the vertical plasma position z of discharges #12868, #24377 and #24375.

Since this piecewise linearization principle follows the time dependent nonlinearities ($C_k^\dagger$ is a function of time) during the discharge, a more accurate state reconstruction is achieved compared with the static state reconstruction given by equation (40), i.e.

$$\check{x}_p(t_k) = C_0^\dagger y_{\mathrm{md}}(t_k). \tag{42}$$

We analyse the state reconstruction robustness of the following four cases.

(i) Variation of the elongation κ (discharge #12868). The $C_0^\dagger$ matrix is evaluated at $t_0 = 0.4$ s. The comparison of the unstable state reconstruction $\hat{x}_1$ with the nonlinear time dependent state reconstruction (NTDSR) references is depicted in figure 11(i). The state reconstruction perfectly fits the reference in the neighbourhood of the linearization equilibrium at $t_0 = 0.4$ s. The accuracy gets slightly worse when the elongation κ and the plasma current I_p differ significantly from the corresponding values at the linearization equilibrium times (0.1–0.2 s and around 0.7 s). Nevertheless, the state reconstruction can be assessed as surprisingly accurate for the whole discharge.

(ii) Variation of the vertical plasma position z (discharge #24377). The $C_0^\dagger$ matrix is taken at $t_0 = 0.55$ s. The comparison of the unstable state reconstruction $\hat{x}_1$ with the NTDSR references is depicted in figure 11(ii). Again, the state reconstruction fits the reference perfectly in the neighbourhood of the linearization equilibrium at t_0. The accuracy gets slightly worse during the upper and the lower knees of the z evolution, where the state reconstruction is slightly underestimated compared with the reference in both cases.

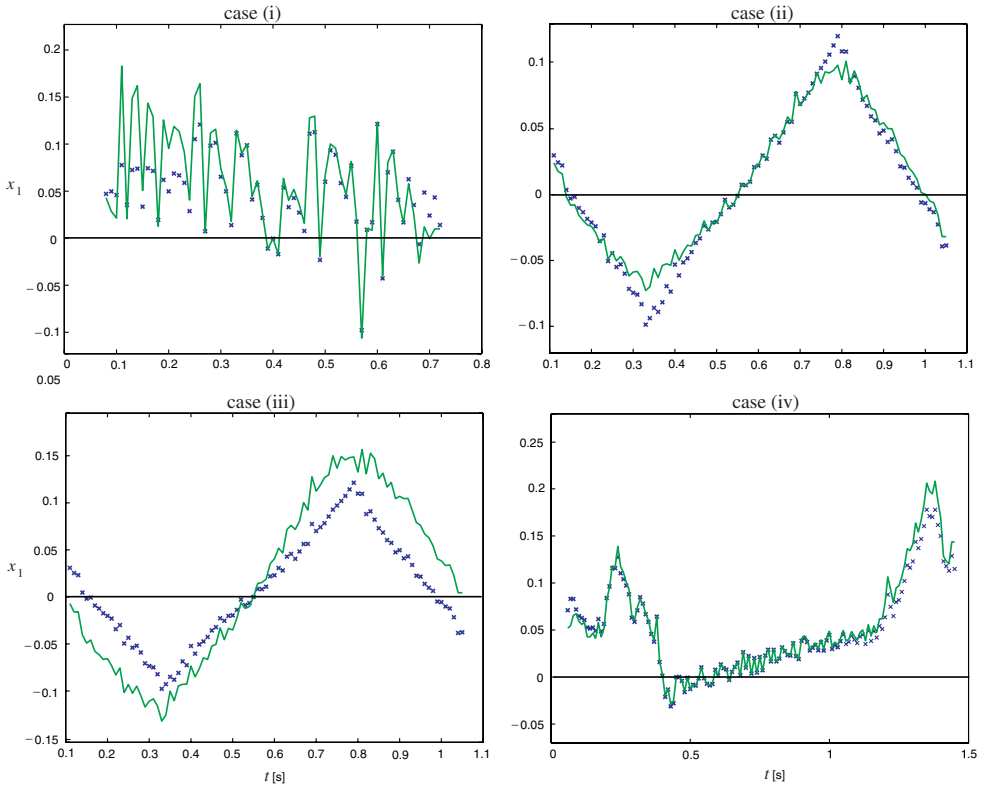

Figure 11. Reconstruction of the unstable state $\hat{x}_1$. Green solid: state reconstruction; blue x: NTDSR reference. (i): during the variation of κ (discharge #12868), (ii): during the variation of z (discharge #24377), (iii): during the variation of z (discharge #24377) with reconstruction C matrix of discharge #24375, (iv): during the ramp-up and ramp-down of I_p (discharge #24375).

(iii) Variation of the vertical plasma position z (#24377) with a state reconstruction matrix $C_0^\dagger$ derived from a similar discharge (discharge #24375) without any variation of the plasma parameters. The $C_0^\dagger$ matrix is taken from discharge #24375 at $t = 0.55$ s, while the NTDSR reference is derived from discharge #24377. The comparison of the unstable state reconstruction $\hat{x}_1$ against the NTDSR references is depicted in figure 11(iii). This time there is a pronounced discrepancy between the slopes of the state reconstruction and the NTDSR reference. This is due to a static gain error of the C matrices (and thus of the $C^\dagger$ matrices) between the linear model derived from discharge #24375 and the model derived from discharge #24377. In this particular case, this leads to an overestimate of the unstable state compared with the reference although such a reconstruction can also lead to an underestimate.

(iv) Ramp-up and ramp-down of the plasma current I_p (discharge #24375). The $C_0^\dagger$ matrix is taken at $t_0 = 0.55$ s. The comparison of the unstable state reconstruction $\hat{x}_1$ with the LIUQE and the NTDSR references is depicted in figure 11(iv). The state reconstruction is again surprisingly accurate for the whole discharge.

For the analysis of the ramp-up and the ramp-down of a discharge, RZIP models have to be derived during the ramps, for example from a real-time equilibrium reconstruction.

However, LIUQE is not able to provide a reconstruction at the very start of a discharge (during the early ramp-up) and at the very end of a discharge (during the final ramp-down). Since RZIP uses LIUQE results to provide a linear model, there is no linear tokamak model available for a certain time lapse during the initial ramp-up and the final ramp-down.

The robustness study of the state reconstruction can be summarized as follows. The reconstruction with the proposed static least squares error method works well for TCV. Somewhat surprisingly, it seems that it works accurately for a whole discharge, including ramp-up and ramp-down. If we want to apply the reconstructed states to the CNGSC controller then the sole problem that can arise is due to an eventual underestimate of the unstable state x_1. An overestimate is benign, since the controller will still try to stabilize the plasma position more vigorously. Over- or under-estimation can occur when the reconstruction matrix $C_0^\dagger$ is taken from one discharge and applied to another similar discharge (see case (iii)).

6. Conclusion and discussion

A simple CNGSC for the stabilization of the tokamak unstable vertical position in the presence of a radial field power supply voltage saturation is proposed. The principle is to modify an existing linear controller, referred to as the reference controller, by introducing a simple nonlinear term into the control law. This new controller enlarges the RoA to the maximal reachable RoA under input saturation, which is the NCR. Its local performance around the origin is similar to that of the reference controller which will have been optimized using the vast array of linear techniques available. An additional advantage of the nonlinear controller is that the unstable state is brought back faster to the origin for large excursions and, as a result, the rejection of the disturbance is more efficient. This is a benefit of the nonlinear function which forces the controller to concentrate on the control of the unstable state in the proximity of the boundaries of the NCR as well as beyond it. These features have been demonstrated on linearized models of ITER and JET. The algebraic implementation is simple, once an estimate of the unstable state has been obtained.

6.1. Tradeoff between different controllers

There is always a tradeoff between the stability properties and the general controller performance. A standard linear full state feedback controller ($\tilde{u} = fx$) can provide local performance and ac loss reduction but the stability properties are weak since the RoA is smaller than the NCR ($\mathcal{A} \subset \mathcal{C}$). The stability properties can be enhanced by focusing on the feedback of the unstable state. This idea is best represented by considering a linear state feedback controller for which only the unstable state is fed back ($\tilde{u} = f_1 x_1$). For such a controller the enhancement of stability is clear since the RoA is equal to the NCR ($\mathcal{A} = \mathcal{C}$). But since only a single state is fed back the local performance might be lost. The time-optimal DANTOC controller proposed by Scibile [16, 17] was shown to enhance the stability and simultaneously to ensure the local performance. Since it is a bang–bang controller, it handles saturation almost optimally. However, as mentioned in section 3.2, ac losses are minimized by a 'quiet' controller behaviour. We include the impact of the controller choice on ac losses in this tradeoff in table 4. The CNGSC controller proposed in this paper can handle the three requirements: it enhances the stability and can simultaneously take into consideration the local performance and the ac loss reduction.

Table 4. Tradeoff between different controllers.

	Stability properties	Local performance	Ac loss reduction	Application to higher order systems	Simple design
Standard linear feedback controller	Weak $\mathcal{A} \subset \mathcal{C}$	√	√	√	√
Unstable state feedback controller	Enhanced $\mathcal{A} = \mathcal{C}$	—	√	√	√
Near time optimal VSC controller DANTOC, [16, 17]	Enhanced $\mathcal{A} = \mathcal{C}$	√	—	— Has to be investigated	—
CNGSC controller	Enhanced $\mathcal{A} = \mathcal{C}$	√	√	√	√

All controllers except for the DANTOC controller are applicable to arbitrary high order systems and the controller design remains simple, but the DANTOC controller has not yet been applied to systems of higher order than two.

From this tradeoff discussion we see that incorporating the unstable state into the control law is essential for enhancing the stability of a tokamak closed-loop system.

The approach presented in this paper for controlling an unstable mode is equally applicable to the resistive wall mode. The major challenge in applying this technique to both the vertical position stabilization and the resistive wall mode stabilization is an accurate estimate of the evolution of the unstable state itself for which we have explained the problem and proposed a suitable approach. Work is presently underway to implement the proposed state reconstruction method in nonlinear simulations of the vertical position control problem.

The distinction between the growth of the unstable mode and the evolution of the vertical movement has not yet attracted enough attention. The stable mode of the system can pollute the estimate of the position by polluting the diagnostic measurements, if these are not adequately compensated in the estimate. The vertical movement is not a pure exponential but contains contributions from the decaying stable modes. The experimental paradox is that at short times these modes are strongest, since they have not decayed, whereas at short times the exponential is most likely to be pure due to a valid local linearization. When comparing experimentally estimated growth rates with the unstable eigenmode eigenvalue, care should be taken in considering this point and in considering to what accuracy models are really validated.

Improving the quality of the estimate of the unstable mode amplitude appears to be a more severe challenge than had been imagined. This work is beyond this paper, which has only been able to illustrate the problems encountered and the approach made. The use of the loop-voltage measurements also needs to be investigated in detail.

Acknowledgments

This work was carried out in collaboration with many colleagues working on ITER control. We are specifically grateful to R Albanese, Y Gribov, A Kavin, A Portone and F Villone for providing us the access to the JET and ITER plasma equilibrium response models and

controllers. The work was partly supported by the Swiss National Science Foundation. The continued support by Professor D Bonvin was essential.

Appendix A. Normalization of the tokamak closed-loop system

This appendix describes the tokamak closed-loop system for controller design. A full description of this appendix can be found in [12].

Appendix A.1. The tokamak closed-loop system for controller design

For controller design we consider a tokamak closed-loop system composed of the following three parts (figure A1):

(i) The linear tokamak model: the typical tokamak linear model (RZIP or CREATE-L) consists of 50–100 state variables $x_p \in \mathbb{R}^{n_p}$, several PF coils and their voltage inputs and several outputs $y_p \in \mathbb{R}^{m_p}$. Since there are two different controllers, the inputs are divided into two parts: (i) the vertical stabilization control input $u_{\mathrm{vc}} \in \mathbb{R}$ and (ii) the plasma shape control input $u_{\mathrm{sc}} \in \mathbb{R}^{k_p}$. The resulting linear tokamak model is given by

$$\begin{aligned} \dot{x}_p &= A_p x_p + B_{p_{\mathrm{sc}}} u_{\mathrm{sc}} + B_{p_{\mathrm{vc}}} u_{\mathrm{vc}} + E_p \dot{w}, \\ y_p &= C_p x_p + F_p w, \\ y &= C_{p_y} x_p + F_{p_y} w, \\ z &= C_{p_z} x_p + F_{p_z} w. \end{aligned} \tag{A.1}$$

Note that the output y_p includes both the magnetic diagnostic measurements and the plasma parameters. The outputs $y \in \mathbb{R}^{m_{\mathrm{sc}}}$ and $z \in \mathbb{R}^{m_{\mathrm{vc}}}$ are output subsets of y_p. The outputs y (i.e. z, R, g and I_p) are needed for the plasma shape control, while z is needed for the vertical stabilizing control. For the stabilizing controller the vertical position of the plasma z is usually used and that is why we denote this output as z. But note that we could also use an output other than the vertical plasma position for the vertical stabilization control. The important thing is that z has to be a single output. Note that z is normally a member of y or a linear combination of y.

(ii) The plasma shape controller and power supplies (SC): in general, the plasma shape controller is a low order controller which only controls the slow movement of the plasma equilibrium. There are several inputs $y \in \mathbb{R}^{k_{\mathrm{sc}}}$ and outputs $\tilde{u}_{\mathrm{sc}} \in \mathbb{R}^{m_{\mathrm{sc}}}$. Each output drives a single power supply and each power supply possesses a voltage saturation with a saturation level denoted as σ_{sc}, where each $i \in 1 \ldots m_{\mathrm{sc}}$ corresponds to a power supply. The controller can be any stable and proper system which is described by

$$\begin{aligned} \dot{x}_{\mathrm{sc}} &= A_{\mathrm{sc}} x_{\mathrm{sc}} + B_{\mathrm{sc}} y \\ \tilde{u}_{\mathrm{sc}} &= C_{\mathrm{sc}} x_{\mathrm{sc}} + D_{\mathrm{sc}} y. \end{aligned} \tag{A.2}$$

Note that if we want to implement a PID controller then we have to add a low-pass filter into the derivative part D to satisfy the condition of a proper system.

(iii) The vertical stabilizing controller and power supply (VC): similar to the plasma shape controller, the vertical stabilizing controller can be any stable and proper system with a single input z and a single output $\tilde{u}_{\mathrm{vc}}$ which is described by

$$\begin{aligned} \dot{x}_{\mathrm{vc}} &= A_{\mathrm{vc}} x_{\mathrm{vc}} + B_{\mathrm{vc}} z, \\ \tilde{u}_{\mathrm{vc}} &= C_{\mathrm{vc}} x_{\mathrm{vc}} + D_{\mathrm{vc}} z. \end{aligned} \tag{A.3}$$

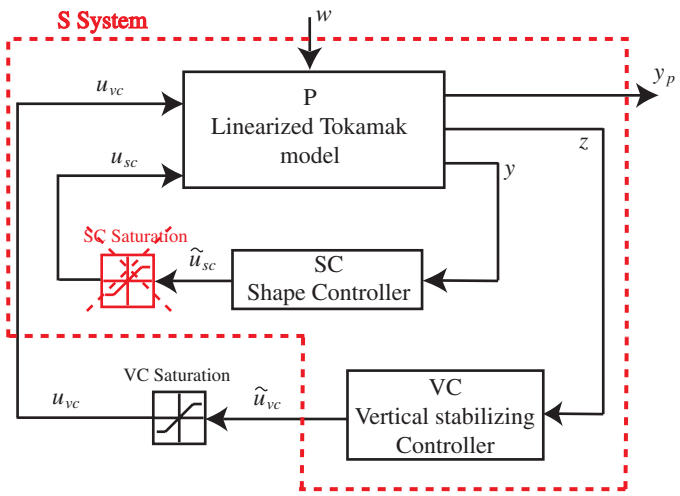

Figure A1. Illustration of the tokamak closed-loop system. Transformation of the tokamak closed-loop system by unifying the linearized tokamak model, the SC and the VC controllers (blocks enclosed by the dashed frame). The SC saturation is ignored.

In practice, the vertical stabilizing controllers are often simple PD or pure D controllers. The single power supply possesses a voltage saturation with a saturation level denoted by σ_{vc}.

Appendix A.2. Design considerations for the SC and VC controllers

In this paper we consider the stabilization problem with a single saturated input, namely the saturation of the single power supply driven by the VC controller. We therefore assume that the SC and VC controllers are completely decoupled in terms of stabilization. Only the VC controller should have a stabilizing effect, i.e. an effect on the unstable state, while the SC controller has to be designed such as to have little or no effect on the unstable state. A possible effect of the SC controller on the stabilization can be verified by computing the eigenvalues of the closed-loop system composed of the tokamak linear model and the SC controller only. If there is a positive eigenvalue which is approximately equal to the positive eigenvalue of the linear tokamak model, then in general it can be assumed that SC controller only has a weak effect on the stabilization. Nevertheless, this condition must not result from a combination which consists of eliminating the original unstable mode of the tokamak and simultaneously introducing a new unstable mode. Knowledge of how to decouple the vertical stabilizing control part from the plasma shape control part is therefore indispensable. In what follows we suppose that the SC and VC controllers are well conditioned, so only the VC controller has an impact on the stability of the closed-loop system.

Appendix A.3. Transformation and normalization of the tokamak closed-loop system

For the purpose of the analysis and the synthesis of an improved VC controller, it is necessary to transform and to normalize the tokamak closed-loop system. The first step unifies the linearized tokamak model and the SC controller into a linear system. We realistically assume that the SC controller never saturates its power supplies during a plasma disturbance and thus

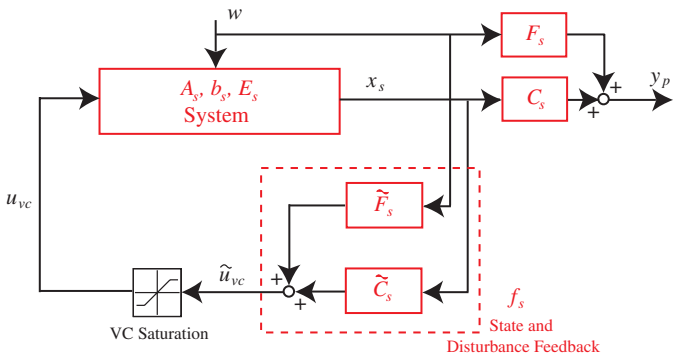

Figure A2. The S system and the state and disturbance feedback.

we ignore the SC saturation (see figure A1). The second major transformation step consists of substituting the input–output VC controller into a state feedback controller. Both steps are carried out by calculating the transfer function from the input u_{vc} to the output $\tilde{u}_{\mathrm{vc}}$, i.e. by unifying the tokamak model, the SC and the VC controllers (blocks enclosed by the dashed frame in figure A1) into a single system, referred to as the S system. This new S system is given by

$$\begin{aligned} \dot{x}_s &= A_s x_s + b_s u_{\mathrm{vc}} + E_s w, \\ y_p &= C_s x_s + F_s w, \\ \tilde{u}_{\mathrm{vc}} &= \tilde{C}_s x_s + \tilde{F}_s w, \end{aligned} \tag{A.4}$$

where we assume that the resulting state vector containing the state vectors of the three systems is defined as

$$x_s = \begin{bmatrix} x_p \\ x_{\mathrm{sc}} \\ x_{\mathrm{vc}} \end{bmatrix} \in \mathbb{R}^n. \tag{A.5}$$

The resulting tokamak closed-loop system is illustrated in figure A2. The state output matrix $\tilde{C}_s$ can be interpreted as a state feedback controller. Because of the disturbance w and the matrix F_p, we have to add a disturbance feedback part denoted as $\tilde{F}_s$. We therefore define the state feedback gain as $f_s = [\tilde{C}_s \quad \tilde{F}_s]$ and the state feedback leads to

$$\tilde{u}_{\mathrm{vc}} = \begin{bmatrix} \tilde{C}_s & \tilde{F}_s \end{bmatrix} \begin{bmatrix} x_s \\ w \end{bmatrix} = f_s \begin{bmatrix} x_s \\ w \end{bmatrix}. \tag{A.6}$$

The last transformation step consists of normalizing the S system by diagonalizing the A_s matrix and by replacing the VC saturation by the normalized saturation function defined by

$$u = \mathrm{sat}(\tilde{u}) = \begin{cases} -1 & \text{if } \tilde{u} < -1, \\ \tilde{u} & \text{if } -1 \leqslant \tilde{u} \leqslant 1, \\ 1 & \text{if } \tilde{u} > 1. \end{cases} \tag{A.7}$$

This is achieved by the linear state transformation

$$x = T^{-1} x_s. \tag{A.8}$$

The resulting normalized system becomes

$$\begin{aligned} \dot{x} &= Ax + bu + E\dot{w} \\ y_p &= Cx + Fw \\ \tilde{u} &= \tilde{C}x + \tilde{F}w, \end{aligned} \tag{A.9}$$

where

$$A = T^{-1}A_sT, \qquad b = T^{-1}b_s, \qquad E = T^{-1}E_s, \qquad C = C_sT,$$
$$F = F_s, \qquad \tilde{C} = \tilde{C}_sT \qquad \text{and} \qquad \tilde{F} = \tilde{F}_s.$$

The linear transformation matrix T is derived by means of a modified eigenvalue and eigenvector decomposition where we impose an orthogonal A matrix such that the diagonal elements of matrix A are the real parts of the eigenvalues of A_s (and thus A), i.e.

$$A = T^{-1}A_sT = \begin{bmatrix} \lambda_1 & 0 & 0 & \cdots & 0 & 0 & \cdots & 0 \\ 0 & \lambda_2 & 0 & \cdots & 0 & 0 & \cdots & 0 \\ 0 & 0 & \lambda_3 & \cdots & 0 & 0 & \cdots & 0 \\ \vdots & \vdots & \vdots & \ddots & \vdots & \vdots & \vdots & \vdots \\ 0 & 0 & 0 & \cdots & \lambda_r & \mu_r\nu_r & \cdots & 0 \\ 0 & 0 & 0 & \cdots & -\mu_r/\nu_r & \lambda_r & \cdots & 0 \\ \vdots & \vdots & \vdots & \vdots & \vdots & \vdots & \ddots & \vdots \\ 0 & 0 & 0 & \cdots & 0 & 0 & \cdots & \lambda_{n_c} \end{bmatrix}, \tag{A.10}$$

where $\lambda_1 > 0$ is the unstable pole and $0 > \lambda_2 \geqslant \lambda_3 \geqslant \ldots \geqslant \lambda_{n_c}$ are the real parts of the stable poles, where $n_c \leqslant n$. Conjugate complex pole pairs (i.e. $\lambda_r \pm j\mu_r$) are represented as square submatrices, where $\nu_r \in \mathbb{R}$ can be an arbitrary chosen value. Furthermore,

$$b = T^{-1}b_s = \begin{bmatrix} \lambda_1 & \lambda_2 & \lambda_3 & \cdots & b_{r_1} & b_{r_2} & \cdots & \lambda_{n_c} \end{bmatrix}^{\mathrm{T}}, \tag{A.11}$$

where b_{r_1}, b_{r_2} and also ν_r are given by imposing $A^{-1}b = [1 \quad 1 \quad \ldots \quad 1]$.

Similar to the S system (equation (A.4)), the state output matrix $\tilde{C}$ is interpreted as a state feedback controller. Again we have to add the part due to the disturbance input w and for which $\tilde{F}$ represents the disturbance feedback, and we therefore again interpret the disturbance w as a state of the system. We define the state feedback gain as

$$f = [f_1 \quad f_2 \quad \ldots \quad f_n] = \tilde{C} \tag{A.12}$$

and the disturbance feedback gain as

$$f_w = [f_{w_1} \quad f_{w_2} \quad \ldots \quad f_{w_{l_p}}] = \tilde{F}. \tag{A.13}$$

The significant advantage of this somewhat longwinded state orthogonalization is that such a system can now immediately be subdivided into two independent subsystems, i.e. [15]

$$\begin{bmatrix} \dot{x}_1 \\ \dot{x}_{\mathrm{st}} \end{bmatrix} = \begin{bmatrix} \lambda_1 & 0 \\ 0 & A_{\mathrm{st}} \end{bmatrix} \begin{bmatrix} x_1 \\ x_{\mathrm{st}} \end{bmatrix} + \begin{bmatrix} \lambda_1 \\ b_{\mathrm{st}} \end{bmatrix} u, \tag{A.14}$$

where $x_1 \in \mathbb{R}$ and λ_1 describe the unstable subsystem and $x_{\mathrm{st}} = [x_2 \quad x_3 \quad \ldots \quad x_n]^{\mathrm{T}} \in \mathbb{R}^{n-1}$, A_{st} and b_{st} describe the stable subsystem.

Appendix B. Shifting of the NCR during a disturbance

Consider the normalized system (equation (20)), i.e.

$$\dot{x} = Ax + bu + E\dot{w}.$$

In section 2.4 (see also figure 1) we defined the derivative of the ELM-like disturbance, $\dot{w}$, as piecewise constant. Thus, we define a piecewise constant disturbance input $\bar{d} \in \mathbb{R}^n$, i.e.

$$\bar{d} = E\dot{w} \tag{B.1}$$

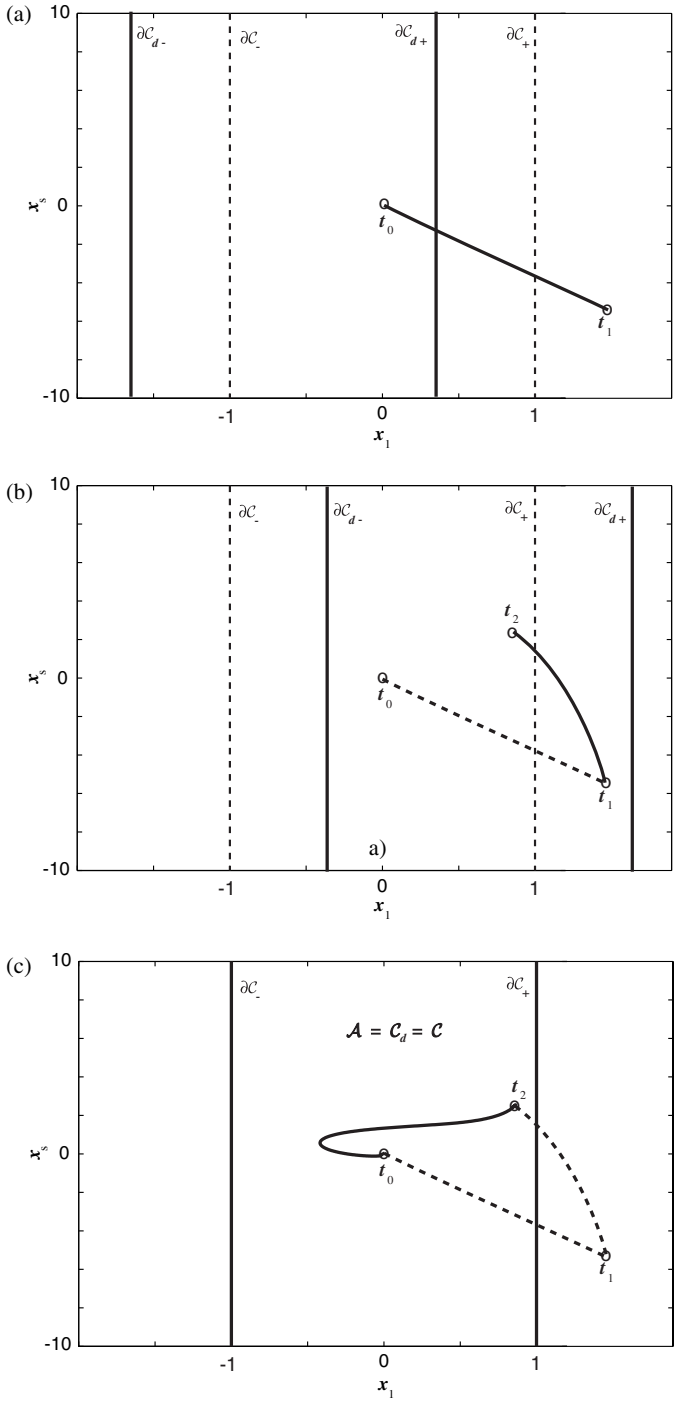

Figure B1. The shifting of the NCR during a disturbance: (*a*) $t_0 < t < t_1$, (*b*) $t_1 < t < t_2$ and (*c*) $t_2 > t$ (same disturbance as in figure 8).

leading to the system

$$\dot{x} = Ax + bu + \bar{d}. \tag{B.2}$$

By the state transformation

$$\tilde{x} = x + A^{-1}\bar{d} \tag{B.3}$$

and by noticing that the derivative of $A^{-1}\bar{d}$ is zero since $\bar{d}$ is piecewise constant we obtain a system without any disturbance input, i.e.

$$\dot{\tilde{x}} = A\tilde{x} + bu. \tag{B.4}$$

For a system without a disturbance input the NCR is trivially given by definition (30), i.e.

$$\tilde{\mathcal{C}} = \{\tilde{x} \in \mathbb{R}^n : |\tilde{x}_1| < 1\}.$$

Therefore, we can apply the state translation (B.3) to the unstable state, i.e. $\tilde{x}_1 = x_1 + \bar{d}_1/\lambda_1$, where d_1 is the disturbance input for the unstable state and $1/\lambda_1$ is due to the inversion of the diagonalized matrix A. In this way we obtain the NCR of the system with disturbance input (equation (B.2)):

$$\mathcal{C}_d = \left\{ x \in \mathbb{R}^n : \left| x_1 + \frac{\bar{d}_1}{\lambda_1} \right| < 1 \right\}.$$

We conclude that during a disturbance the NCR is shifted as a function of the constant piecewise disturbance input $\bar{d}_1$. Figure B1(a) shows the trajectory evolution during the drop phase of the disturbance ($t_0 < t < t_1$) where $\bar{d}_1 > 0$. The NCR $\mathcal{C}_d$ is shifted to the left (negative part) in the unstable state-space and the trajectory inevitably leaves the NCR. During the recovery time of the disturbance ($t_1 < t < t_2$) where $\bar{d}_1 < 0$ the NCR $\mathcal{C}_d$ is shifted to the right (positive part) in the unstable state-space with the consequence that the trajectory is now located inside the NCR $\mathcal{C}_d$ (figure B1(b)). Thus, the trajectory is no longer diverging and can be steered towards the origin. After the disturbance has vanished ($t_2 < t$) we can again consider the system without a disturbance (figure B1(c)). In this case the trajectory is located inside the NCR $\mathcal{C}_d = \mathcal{C}$ and since for the CNGSC controller the RoA is equal to the NCR the trajectory is steered back to the origin.

References

[1] ITER Physics Basis Editors 1999 The ITER physics basis. *Nucl. Fusion* **39** 2137–670

[2] Bertolini E, Mondino P L and Noll P 1987 The JET magnet power supplies and plasma control systems *Fusion Technol.* **11** 71–119

[3] Lazarus E A, Lister J B and Neilson G H 1990 Control of the vertical instability in tokamaks *Nucl. Fusion* **30** 111–41

[4] Lister J B *et al* 1990 Experimental study of the vertical stability of high decay index plasmas in the DIII-D tokamak *Nucl. Fusion* **30** 2349–66

[5] Villone F, Vyas P, Lister J B and Albanese R 1997 Comparison of the CREATE-L plasma response model with TCV limited discharges *Nucl. Fusion* **37** 1395–410

[6] Vyas P, Villone F, Lister J B and Albanese R 1998 The separatrix response of diverted TCV plasmas compared with the predictions of the CREATE-L model *Nucl. Fusion* **38** 1043–53

[7] Coutlis A, Bandyopadhyay I, Lister J B, Vyas P, Albanese R, Limebeer D J N, Villone F and Wainwright J P 1999 Measurement of the open loop plasma equilibrium response in TCV *Nucl. Fusion* **39** 663–84

[8] Lister J B, Sharma A, Limebeer D J N, Nakamura Y, Wainwright J P and Yoshino R 2002 Plasma equilibrium response modelling and validation on JT-60U *Nucl. Fusion* **42** 708–24

[9] Hofmann F, Moret J-M and Ward D J 1998 Stability analysis of the vertical position control loop in TCV using rigid and deformable plasma models *Nucl. Fusion* **38** 1767–78

[10] Jardin S C, Pomphrez N and DeLucia J 1986 Dynamic modelling of transport and positional control in a tokamak *J. Comput. Phys.* **66** 481

[11] Khayrutdinov R R and Lukash V E 1993 Studies of plasma equilibrium and transport in a tokamak fusion device with the inverse-variable technique *J. Comput. Phys.* **109** 193–201
[12] Favez J-Y 2004 Enhancing the control of tokamaks via a continuous nonlinear control law *PhD Thesis* No 3034, École Polytechnique Fédérale de Lausanne-Switzerland http://crppwww.epfl.ch/archives
[13] Albanese R and Villone F 1998 The linearized CREATE-L plasma response model for the control of current, position and shape in tokamaks *Nucl. Fusion* **38** 723–38
[14] Kavin A 2000 ITER-FEAT linear models description *ITER NAKA JWS, Issue 1 (Naka, Japan, 10 July 2000)*
[15] Hu T and Lin Z 2000 *Control Systems with Actuator Saturation: Analyses and Design* (Boston: Birkhauser)
[16] Scibile L and Kouvaritakis B 2000 Stability region for a class of open-loop unstable linear systems: theory and application *Automatica* **36** 37–44
[17] Scibile L 1997 Nonlinear control of plasma vertical position in a tokamak *PhD Thesis* University of Oxford
[18] Schärz B, Bruzzone P, Favez J-Y, Lister J B and Zapretilina E 2001 The effect of the feedback controller on superconducting tokamak AC losses, LRP 714, CRPP, Switzerland
[19] Alvarez J, Suárez R and Alvarez J 1993 Planar linear systems with single saturated feedback *Syst. Control Lett.* **20** 319–26
[20] Hu T, Lin Z and Qiu L 2001 Stabilization of exponentially unstable linear systems with saturating actuators *IEEE Trans. Automat. Control* **46** 973–9
[21] Pinch E R 1993 *Optimal Control and the Calculus of Variations* (New York: Oxford University Press)
[22] Favez J-Y, Mullhaupt Ph, Srinivasan B and Bonvin D 2004 A Globally stabilising controller under saturated input for linear planar systems with one unstable pole *ACC 2004: American Control Conf. (Boston, USA)*
[23] Ariola M, Pironti A and Portone A 2000 Vertical stabilization and plasma shape control in the ITER-FEAT tokamak *Proc. 2000 IEEE Int. Conf. on Control Applications (Anchorage, Alaska, USA, 2000)* pp 401–5
[24] Albanese R, Calabrò G, Mattei M and Villone F 2003 Plasma response models for current, shape and position control in JET *Fusion Eng. Des.* 66–8
Albanese R, Calabrò G, Mattei M and Villone F 2003 Plasma response models for current, shape and position control in JET *Fusion Eng. Des.* **66–68** 715–18
[25] Hofmann F and Tonetti G 1988 Tokamak equilibrium reconstruction using Faraday rotation measurements *Nucl. Fusion* **28** 1871–8